Han, S., Xie, L., Du, X., Xiang, C., Huang, J., Tang, Z., Wang, C., Horsfield, B., Mahlstedt, N. (2023): Insights into organic metagenesis using Raman spectroscopy and high resolution mass spectrometry: A case study of the Shahezi formation, deep Songliao basin, China. - International Journal of Coal Geology, 265, 104153.

https://doi.org/10.1016/j.coal.2022.104153

Insights into organic metagenesis using Raman spectroscopy and high resolution mass spectrometry: a case study of the Shahezi formation, deep Songliao basin, China

Shuangbiao Han[a*], Linfeng Xie[a], Xin Du[a], Chaohan Xiang[a], Jie Huang[a], Zhiyuan Tang[a], Chengshan Wang[b], Brian Horsfield[c], Nicolaj Mahlstedt[c]

a. College of Geoscience and Surveying Engineering, China University of Mining and Technology, Beijing 100083, China
b. State Key Laboratory of Biogeology and Environmental Geology, China University of Geosciences, Beijing 100083, China
c. German Research Centre for Geosciences, Potsdam, Brandenburg 14473, Germany
* Corresponding author: bjcuphan@163.com

Abstract

The maturity of sedimentary organic matter is a key parameter for evaluating oil and gas resources. Existing maturity indicators have different evaluation principles and application scopes. This study investigated samples of high to overmature lacustrine source rocks (Ro = 1.33%-4.24%) from the deep Shahezi formation in the Songliao basin, including the zone of catagenesis and metagenesis. Various methods, including vitrinite reflectance, Tmax, laser Raman spectroscopy, and Fourier transform ion cyclotron resonance mass spectrometry (FT-ICR MS) were used to evaluate the samples' maturity. Through laser Raman analysis of representative samples from the Shahezi formation, most laser Raman parameters showed an inflection point or reversal when the thermal evolution of deep source rocks in the Shahezi formation reaches a certain stage. The variation trend of some Raman parameters and Ro has strong regularity (1.33%<Ro<3.52%). Based on FT-ICR MS, this research analyzed the relative content and molecular composition of polycyclic and heterocyclic aromatic compounds in soluble organic matter of lake source rock samples and comparison samples (marine shale). Quantitative maturity evaluation of organic matter was performed by converting

the signal intensity of each compound. The fitting results of maturity parameter based on FT-ICR MS and Tmax indicated that the maturity parameter of the samples have high coefficient of correlations with maturity in the vitrinite reflectance (Ro) range of 1.33%-2.5% and the Tmax range of 420 °C-600 °C. The maturity parameter values decreased as Ro exceeded 2.5% and Tmax exceeded 600 °C. These findings are attributed to the thermal stability of organic compounds and the formation of pyrobitumen and graphite. The parameters of laser Raman spectroscopy also confirmed the growth of aromatic rings reflected by the maturity parameters of FT-ICR MS. These two methods revealed the structural changes of organic matter in the thermal evolution process from multiple perspectives and provided insights for the maturity evaluation of deep source rocks.

Keywords: Maturity parameter; Organic compounds; Laser Raman spectroscopy; FT-ICR MS; Songliao basin

1 Introduction

Maturity refers to the thermal evolution degree of organic matter in source rocks, driven principally by time and temperature, and accompanied by the transformation of kerogen into oil, gas and highly carbonaceous residue. It is a critical geochemical parameter for conventional oil and gas exploration as well as shale evaluation because maturity level directly affects the quantity and quality of the generated products(Jarvie et al., 2007; Vandenbroucke and Largeau, 2007). Additionally, organic matter maturity affects the reservoir characteristics of shale(Loucks et al., 2012). Therefore, the accurate assessment of maturity level is a crucial component of exploration protocols for hydrocarbon resources in general.

Maturity evaluation relies upon a multiparameter approach, and uses results gathered at petrographic through molecular scales. At the coarsest scale, organic petrological analysis utilizes reflected light, transmitted light and fluorescence measurements. Vitrinite reflectance (Ro) is a traditional maturity evaluation method

(Burgess, 1977; Staplin, 1969; Teichmüller and Durand, 1983) utilising lignocellulose-derived phytoclasts, and is applied ubiquitously on post-Devonian shales. It is not suitable for the maturity evaluation of older sediments in which land plants (the source of the vitrinite) are absent. For Lower Paleozoic and Proterozoic marine hydrocarbon source rocks, deposited prior to the evolution of land plants, alternative petrographic methods are available, such as marine vitrinite reflectance (R_M^o), bitumen reflectance (BRo), and graptolite reflectance (GRo) (Bertrand and Malo, 2001; Luo et al., 2017; Sanei et al., 2015; Valentine et al., 2014; Xiao and Wu, 1995). The bulk-flow pyrolysis peak temperature for any given heating rate increases as thermally labile substituents are stripped from kerogen in evolving maturation series(Barker, 1974; Espitalié et al., 1977), though values are also controlled by other factors(Yang and Horsfield, 2020).

The biomarkers have been widely used for evaluating organic matter maturity(Boreham et al., 1988; Gentzis et al., 1993; Hatch et al., 1984; Mackenzie et al., 1981; Radke, 1982; Seifert and Moldowan, 1978, 1980; Veld et al., 1993). When the degree of thermal evolution of organic matter gradually increases, compounds with better thermal stability will gradually replace compounds with poor thermal stability. The biomarker parameters are based on the relative concentration of reactants and products to evaluate maturity(Mackenzie et al., 1982; Mackenzie et al., 1981). Ideally, when the maturity reaches a certain level, the biomarker parameter increases from 0 to 1, and then does not change as the thermal evolution continues, making it difficult to indicate the maturity of the organic matter at a higher thermal evolution stage. At present, the commonly used biomarker parameters are C_{29}-sterane 20S/(20S+20R), ββ/(ββ+αα); C_{32}-hopanes 22S/ (22S+22R), Ts/ (Ts+Tm) (17α(H)-22, 29, 30-trinorhopane (Tm) and 18α(H)-22, 29, 30-trinorhopane (TS)) and methylphenanthrene, dibenzothiophene in aromatic hydrocarbons. Previous studies have reported that C_{32}-hopane 22S/ (22S+22R) will reach an equilibrium value of about 0.6 when Ro is close to 0.6 %. The C_{29}-sterane ββ/ (ββ + αα) parameter reached an equilibrium value (0.7) with the increase of maturity when Ro was 0.9%. When Ro increases to about 1.4 %, the Ts/ (Ts+Tm) ratio can reach to 1(Peters and Moldowan, 1993).

Spectroscopic methods, including Raman, infrared and nuclear magnetic resonance (NMR), can evaluate the maturity of shale, even at high levels of maturation (Henry et al., 2019; Henry et al., 2018; Hinrichs et al., 2014; Lünsdorf, 2016; Sauerer et al., 2017; Schito et al., 2017; Veld et al., 1997; Xiao et al., 2020; Yang et al., 2021; Zeng and Cheng, 1998; Zhou et al., 2014). These methods can reveal the structural change characteristics of organic matter in the thermal evolution process by studying the types and quantities of organic matter compounds, the size, vibration and displacement of organic matter chemical structure. For instance, electron spin resonance has been used to measure the changes in free radical concentration of kerogen during catagenesis, and maturity parameters were developed(Pusey, 1973). An inversion associated with the pairing of free electrons and aromatization was documented for the zone of metagenesis (Horsfield, 1984). Infrared and NMR spectra demonstrate that the cellulose component is easier to decompose during thermal evolution, while lignin structures are more stable (Schenk et al., 1990). Protonated aromatic absorbances in infrared spectra show a reversal associated with increasing average ring numbers of aromatic moieties (Schenk and Horsfield, 1998).

Maturity can be evaluated by measuring the content of different types of compounds in source rocks. Alkylbenzothiophenes are present in highest abundance at low maturity whereas the alkyldibenzothiophenes are most abundant at higher stages of maturity(Santamaría-Orozco et al., 1998). Some studies have shown that the Benzocarbazole Ratio (a / acc) increased over the maturity range studied for the crude oils analyzed , showing excellent correlations with source rock maturity(Horsfield et al., 1998). The concentration of the fluoren-9-ones in the bitumen systematically increases with increasing maturity. Among the carbazoles, dibenzo- and/or naphtho-annellated derivatives become more abundant at higher maturity. Among the naphthalene derivatives, the relative amounts of β-isomers increase with increasing maturity as compared to the α-isomers(Wilkes et al., 1998a; Wilkes et al., 1998b). Aromatic N_1, N_1O_1, and N_1S_1 compounds are preferably formed while the amount of O2 compounds decreases as thermal evolution continues to increase. At the same time,

condensation and aromatization of the acidic NSO compounds increases(Poetz et al., 2014).

In this study, we examine the utility of the maturity parameters based on Fourier transform ion cyclotron resonance mass spectrometry (FT-ICR MS) to include the zone of metagenesis, significantly extending the sample maturity range of the targeted Shahezi formation (lower Cretaceous) to 4.24% Ro from 1.33% Ro. Importantly, here we supplement and improve the corresponding parameters, focusing on the maturity of organic matter to reveal inversions of maturity parameters at very advanced levels of thermal stress. Furthermore, laser Raman spectroscopy is used to extend the target organic matter from soluble bitumen (aromatic HCs, oxygen, nitrogen, sulphur compounds detected using FT-ICR MS) to insoluble kerogen and pyrobitumen, allowing the evolution of aromatic ring systems to be compared.

2 Geological Background

The Songliao basin is located in northeast China. It is 750 km long. 350 km wide. Its main body is located in Heilongjiang Province and Jilin Province, covering the administrative regions of the three northeastern provinces. Some areas in the southwest corner are located in the Inner Mongolia Autonomous Region and Liaoning Province. The basin is bordered on the west by the Daxing'an mountains and Bohai Bay basin and on the east by Zhang Guangcai mountains and Xiao Xing'an mountains (Qi'an et al., 2016; Sorokin et al., 2013; Wei et al., 2010). The sedimentary time of the Songliao basin in the Cretaceous period is 86 Ma, and the sedimentary area in the Late Cretaceous period covers 26×10^4 km^2. It is a very large lake basin with the longest development history worldwide. The basin is filled with fine-grained detrital deposits, and lacustrine fine-grained clastic deposits are dominant. The terrain of the Songliao basin is high at the boundary and low in the center, with a north-north-east orientation and a diamond-shaped basin floor.

The Songliao basin is the largest petroleum-bearing continental basin globally and a main continental hydrocarbon-generating basin in China (Chen et al., 2000; Wang et

al., 2013). Most oil and gas sources are located in its central depression. Studies have indicated various types of source rocks with type I, II, and III kerogens in the Songliao basin. The hydrocarbon source rocks in the Songliao basin have a high organic matter content, and the total organic carbon content (TOC) of shale in the Shahezi formation is generally higher than 2% (Cui et al., 2020).

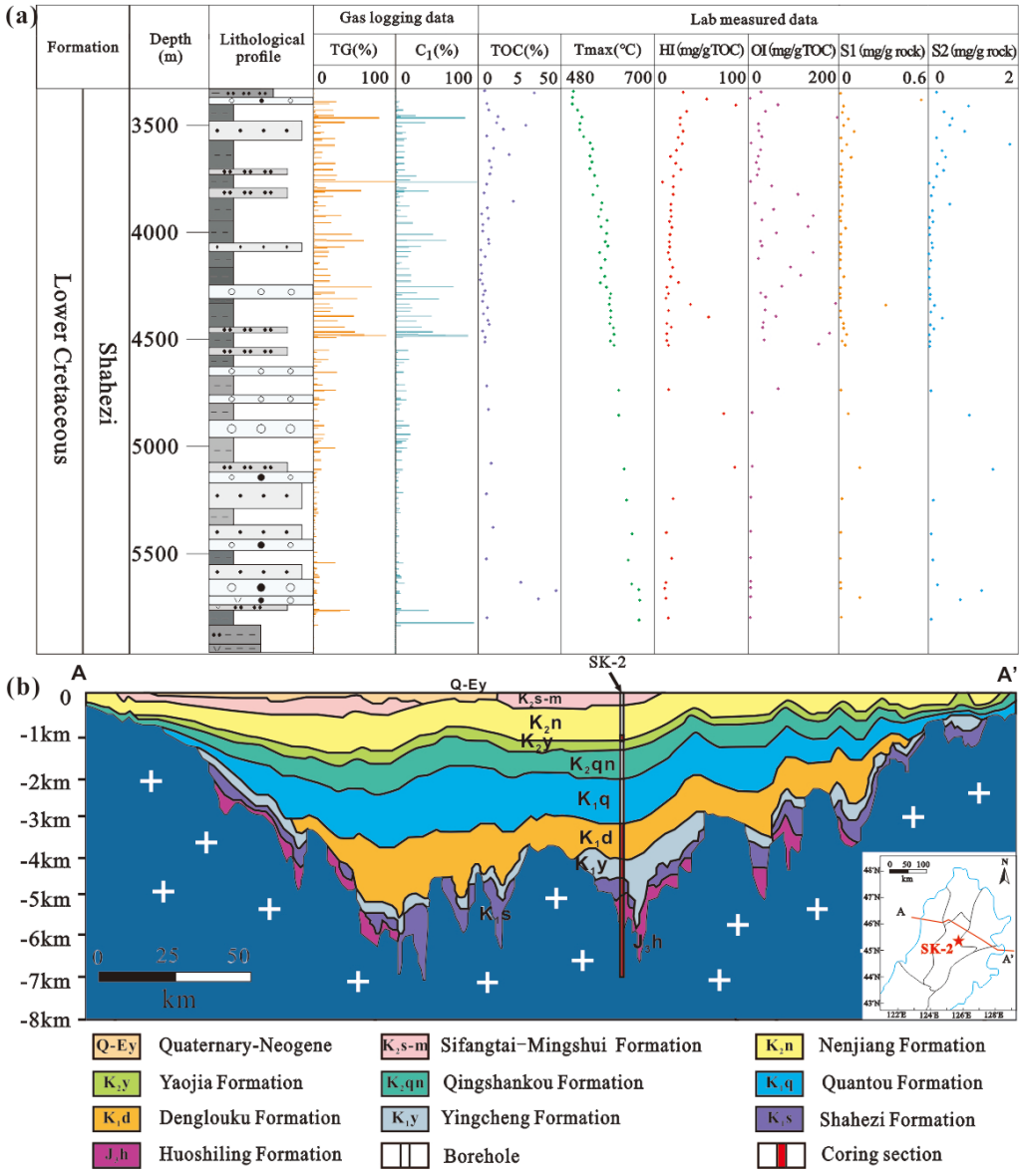

Fig. 1. The location and comprehensive column of continental scientific drilling in the Songliao basin. (a)TOC and Rock-eval parameters from Horsfield et al. (2022) (TG: total hydrocarbon value of gas logging, C_1: methane). (b) modified after Hou et al. (2018), the illustration is the geographic location of the SK-2 well

3 Samples and Methodology

3.1 Samples

Well SK2, drilled as part of the International Continental Scientific Drilling Program (ICDP), is located north of the Xujiaweizi fault depression in the Songliao basin. It is the deepest scientific drilling well (7018m) since the establishment of the ICDP (Fig.1). A 4134.81 m long core (Hou et al., 2018), running through the entire Lower Cretaceous Shahezi formation, with a depth span of 2,623 m (within the depth range of 3337 m to 5960 m) was studied here. The source rocks are highly mature to overmature (1.33%-4.24% Ro), and point to late catagenesis to metagenesis stages, providing an excellent homogeneous series for studying maturation. Laboratory simulation results have shown that large amounts of gas are produced in the late-stage thermal evolution of the indigenous organic matter (Gai et al., 2019; Han et al., 2022a; Horsfield et al., 2022; Li et al., 2015; Wu et al., 2019).

We collected 51 core pieces from the Shahezi formation in SK-2 well, covering a depth range from 3346 m to 5664 m. Basic geochemical analysis and comparison of TOC were conducted to obtain rock pyrolysis parameters of the samples. 10 shale samples and 2 coal samples spanning the entire depth range of the Shahezi formation were elected as representative samples of high to overmature lacustrine facies. Optical microscopy, laser Raman analysis and FT-ICR MS were carried out on these 12 samples.

3.2 Total organic carbon content (TOC) and Rock-Eval analysis

The TOC was determined using a Leco SC-632 instrument before the experiment. The sample was ground to a particle size of less than 0.2 mm, and the hydrochloric acid solution was prepared by mixing 1 volume of HCl with 7 volumes of H_2O.Hydrochloric acid is supplied by Applied Petroleum Technology AS (APT) Norway, following the Norwegian Industry Guide to Organic Geochemical Analyses (NIGOGA), 4th Edition. Briefly, dilute hydrochloric acid was added after crushing the sample, followed by mixing and heating the sample in a Leco combustion furnace. The CO_2 content in the

sample was determined by an infrared detector. The Rock-Eval 6 instrument was used for the rock pyrolysis experiment. The initial temperature (300 °C) was maintained for 3 min. Then, the samples were heated to 650 °C at a constant heating rate of 25 °C /min.

3.3 Optical microscopy and laser Raman analysis

The sample was sliced along the direction perpendicular to the bedding plane of the source rock, embedded into epoxy resin, and polished with diamond suspension to obtain a smooth surface. The sample was placed in a dryer for 12 h. The rock samples were embedded in epoxy resin and polished to obtain a smooth surface. The oil and gas industry standard "Method for the determination of Ro in sedimentary rocks" (SY / T 5124-2012) was used to determine the random reflectance (Rr (%)) by non-polarized light and the maximum reflectance (R_{max}) and average reflectance (R_m) by cross-polarized light using a Lecca DM 4P microscope equipped with the Hilgers FOSSIL MOT standard program. Using a 100-fold magnification objective, we calibrated at least 25 measuring points for each sample using the synthetic reflectivity standard (N-LASF46A: Rr = 1.311%).A BrukerSenterra confocal Raman microscope equipped with an OlympusBX51 high-performance confocal optical microscope with 400 L/mm and 1200 L/mm high-resolution gratings was used for the laser Raman test. 12 samples were crushed into 100-200 mesh powders, The excitation wavelength was 532 nm, the laser power was 5 mW, a 100× objective with a numerical aperture of 0.9, and the diameter of the confocal hole was 100 μm.the integration time was 2 s, the accumulation time was 5, and the resolution was 3-5 cm^{-1}. A concave rubber band baseline correction was applied. Additionally, several authors have demonstrated that sample polishing can induce artifacts to Raman spectra of carbonaceous materials, including shale OM (Beyssac et al., 2003; Henry et al., 2018; Lünsdorf, 2016). However, according to ASTM D2797 (ASTM, 2011), polishing to 0.05 μm is a requirement for the petrographic identification of the various OM maceral types evaluated. In order to avoid the influence of polishing on Raman spectroscopy, the laser Raman sample were not polished in this experiment. The organic matter was searched under the microscope for

Raman test, and the measured Raman data were obtained from the organic matter in the original rock. Photographs of samples under an oil immersion monopolar microscope indicates that the macerals of organic matter analyzed by laser Raman spectroscopy are mainly vitrinite and inertinite. Raman spectra of at least three organic matter particles were measured at different locations (spacing of at least ~ 2 μ m) for each sample. The effect of laser heating on each sample point is assessed by comparing optical micrographs of the sample surface before and after Raman measurements. No thermal alteration of the samples was apparent with the experimental conditions used.

A total of 2 Lorentzian peaks are consistent with the Raman spectrum, corresponding to the D and G peaks. The D and G peaks of the Raman spectra of each sample were fitted directly by Origin 8.0 software, without further decomposition, because of the large uncertainty in the splitting process(Court et al., 2007; Henry et al., 2018; Kouketsu et al., 2014; Lupoi et al., 2017; Quirico et al., 2005). The main purpose of this study is to qualitatively discuss the structural changes of aromatic organic matter during thermal evolution by laser Raman spectroscopy and to facilitate direct comparison with published data based on two-peak fitting(Liu et al., 2013; Wang et al., 2015; Zhou et al., 2014). Previous studies have shown that Raman spectroscopy parameters are not affected by different kerogen compositions (mixed type II / III). Even if there is an organic phase rich in amorphous organic matter, Raman spectroscopy may reduce the risk of thermal maturity assessment of source rocks(Schito et al., 2017). Although the various OM macerals possess different degrees of aromaticity in the original shale sample material, the compositional evolution heat-induced to the OM structure progresses along a similar trend for the evaluated AOM, solid bitumen, and vitrinite(Birdwell et al., 2021). Recent papers (Henry et al., 2019; Henry et al., 2018; Lünsdorf et al., 2017) have now demonstrated that complex, ambiguous deconvolution methods of several bands are not needed, and that reliable results can be achieved otherwise. Some studies suggest that there is no need to perform deconvolution if several Raman parameters can be derived from an un-deconvolved spectrum that can track the thermal evolution of OM(Henry et al., 2019).

3.4 Atmospheric pressure photoionization APPI (+) FT-ICR MS Analysis

The resolution of FT-ICR-MS with magnetic field intensity of 12 Tesla (T) can reach 10^{-6} Da, far exceeding the highest requirement (10^{-4} Da) for the theoretical detection of various non-hydrocarbon compounds composed of carbon (12C = 12Da), hydrogen (1H = 1.0078250321Da), nitrogen (14N = 14.0030740052Da), sulfur (32S = 31.97207069Da), oxygen (16O = 15.9949146221Da), and their isotopes (C = 13.0033548378Da). Thus, in this study, the molecular structure of organic matter is determined using FT-ICR-MS to obtain accurate estimates of the compound mass and the isotopic distribution. The linear relationship between the carbon number and the number of equivalent double bonds is used to determine the degree of aromatization and alkylation of the compounds. The compounds are divided into two intervals, and the organic matter maturity is expressed by their relative abundance. The organic matter maturity is quantified by the percentages of the TMIA of each compound.

The source rock samples (30-50 g) were ground to 120 mesh and extracted at 50 °C for 48 h using dichloromethane containing 1% methanol in a Soxhlet apparatus. The extracts were dissolved in a mixture of methanol and hexane (9:1, v/v) to obtain 2 μg/mL of organic matter solution for each sample. Purity of methanol used in this experiment ≥ 99.85%, and the purity of hexane ≥ 99.5 %. Methanol and hexane were supplied by German Research Centre for Geosciences (GFZ). The sample solutions were injected into the atmospheric pressure photoionization (APPI) source with a syringe pump (Hamilton) at a flow rate of 20 μL/h. Ultra-high-resolution mass spectrometry analysis was performed with a 12T cryo-superconducting magnet (Bruker Solarix FT-ICR MS). The operating conditions of the APPI (+) mode was as follows: capillary voltage − 1000 V; collision-induced dissociation voltage (CID) 30 V; dry gas (nitrogen) flow rate 3 L/min, the purity of nitrogen used in the experiment ≥ 99.9 %. temperature 210 °C; atomized gas (nitrogen), 2.3 bar, temperature 350 °C. The spectrum was recorded in broadband mode using a 4 MB dataset. For the target mass spectrum (in the mass range of m/z 147–1200), 200 scans can be superimposed to generate higher quality spectra. Only signals with a signal-to-noise ratio (SNR) ≥ 12

were used in the analysis.

4 Results and Discussion

4.1 Organic matter richness, vitrinite reflectance and maceral types

The TOC results of the deep source rock samples of the Shahezi formation indicate no significant correlation between TOC and burial depth; therefore, the burial depth has a negligible effect on the TOC of high and overmature source rock of Shahezi formation. In general, the TOC of the source rock in Shahezi formation is high (1%-2%), and for some samples very high (20- 44%). The likely reason is that some samples are from coal-bearing strata, with periodic high organic matter enrichment and high TOC values. The pyrolysis hydrocarbon generation potential (S1+S2) values of the samples are 0.32 to 1.81 mg/g, which is relatively low. The main reason is that the deep shales of the Shahezi are highly mature to overmature, and the organic matter is influenced by long-term thermal evolution and tectonics. The evaluation of petroleum generating potential in highly overmature shales using only the pyrolysis hydrocarbon generation potential has certain limitations (Ganz and Kalkreuth, 1987; Huang, 1999; Liang et al., 2009; Peters, 1986).

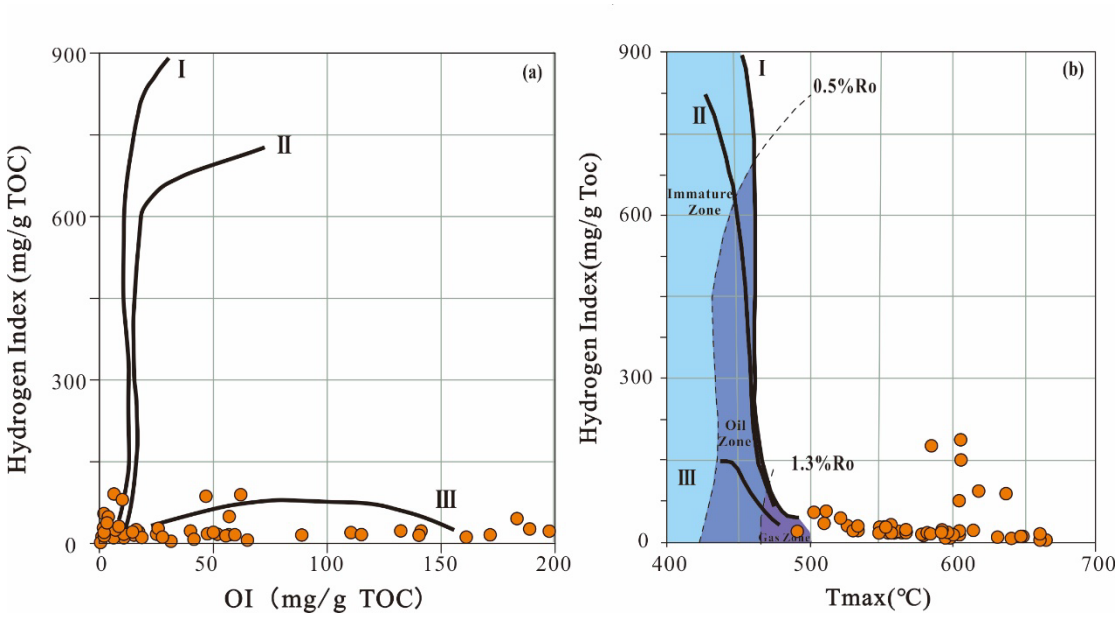

Fig. 2. (a) Hydrogen index versus oxygen index and (b) hydrogen index versus Tmax

(base map is modified according to (Bernard et al., 2012)

The Shahezi formation is located in a lake basin. Since it is controlled by the transgressive system tract, the possible sedimentary organic matter sources are autotrophic bacteria, algae, and terrestrial higher plants. The elemental composition analysis of kerogen shows that the hydrogen index (HI) and oxygen index (OI) of the deep source rock in Well SK-2 are low in the Van Krevelen diagram, and the organic matter type cannot be determined using the two indices (Fig. 2a). In the Tmax-HI diagram, the Tmax values of the deep source rock in Well SK-2 are greater than 500 °C, far beyond the upper limit of the horizontal coordinate, and the type of organic matter cannot be determined (Fig. 2b). The oil-immersion microscopy results of the whole rock slices indicate that the organic matter has a relatively complete wood structure (Fig. 3). Some of it is vitrinite, and some is inertinite. The vitrinite is mainly clastic, with an irregular shape. Most of the inertinite groups are detrital and filamentous with plant sporangium pores.

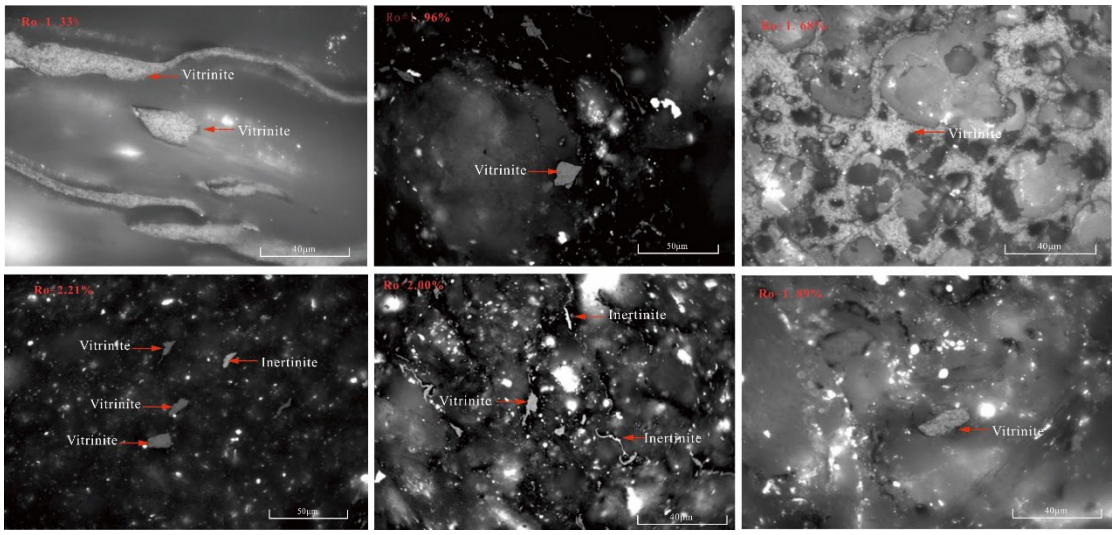

Fig.3. Photographs of samples under an oil immersion monopolar microscope

The Ro and Tmax data of the deep source rock of the Shahezi is positively correlated with the depth (Fig. 1; Table 1.). We use Ro as the classification standard of the mature stage. The Ro of the deep shale samples in the Shahezi formation is greater than 1.3%, and the organic matter is predominantly overmature, with a maximum Ro of 4.24% (5664 m).

In the rock pyrolysis experiment, the part with the worst thermal stability in

kerogen was first thermally degraded. The pyrolysis of kerogen part under pyrolysis needs higher temperature, and Tmax will increase when the maturity of source rock increase. The Tmax data show that the trend of depth-Tmax scatter plot and depth-Ro scatter plot of deep source rock in Shahezi formation is similar, showing a significant positive correlation (Fig. 1). According to the classification standard of mature stage of lacustrine source rocks (SY/T 5735 – 1995), the Tmax of deep source rock samples in Shahezi formation is greater than 500 °C, and the maturity of organic matter is in the high-over mature stage. Among them, the high mature samples and over mature samples account for half, and the Tmax can reach up to 665 °C.

Table 1. TOC and maturity parameters of representative samples of the Shahezi formation. Uncertainties for the Raman parameters represent one standard deviation. Uncertainties for Ro values represent one standard deviation.

Depth(m)	TOC（%）	Tmax (°C)	Ro（%）	Raman parameters（average value）						MAT parameters			
				W_D (cm^{-1})	W_G (cm^{-1})	$D_{(FWHM)}$ (cm^{-1})	$G_{(FWHM)}$ (cm^{-1})	RBS (cm^{-1})	I_D/I_G	CH	O_1	N_1	S_1
3376	20.4	510	1.33±0.06	1345.90±1.24	1588.27±2.78	219.74±5.52	78.19±2.93	242.36±2.18	0.70±0.03	3.04	2.31	2.78	7.75
3466	2.42	533	1.68±0.11	1349.85±3.61	1595.57±5.55	217.55±3.70	82.20±4.80	245.72±1.94	0.56±0.08	3.54	2.94	3.18	7
3586	7.37	552	1.96±0.10	1441.08±60.29	1592.11±3.26	/	70.05±10.47	151.03±57.04	0.66±0.01	4.52	3.92	4.68	9.31
3616	1.85	557	1.89±0.12	1403.94±47.82	1595.83±6.27	/	111.17±2.44	191.89±41.56	0.46±0.04	4.77	4.16	5.03	10.43
3676	1.31	555	2±0.10	1340.52±4.87	1593.33±1.88	230.87±20.66	141.06±43.89	252.81±6.75	0.50±0.08	4.59	4.46	4.79	10.11
3866	4.43	579	2.23±0.15	1354.97±1.90	1595.80±2.22	293.92±6.91	82.82±4.13	240.83±2.22	0.49±0.04	6.01	5.84	5.81	13.24
4426	1.1	597	2.21±0.12	1333.63±1.12	1594.87±0.89	196.01±2.49	57.88±2.45	261.24±0.92	0.63±0.02	5.36	6.1	6.69	9.51
4734	0.97	618	3±0.13	1334.93±2.81	1596.22±3.61	174.68±9.72	60.25±11.74	261.29±6.42	0.61±0.03	4.88	1.36	2.05	1.26
5099	1.56	630	3.33±0.12	1334.31±4.31	1602.13±3.31	174.82±1.20	47.65±2.35	267.82±1.21	0.56±0.03	0.67	1.25	0.44	7.33
5403	1.77	649	3.93±0.10	1331.61±1.12	1602.96±1.05	149.54±4.54	41.10±1.63	271.36±0.74	0.55±0.01	1.01	1.04	0.00	1.13
5523	1.01	640	3.52±0.11	1327.50±3.69	1599.97±4.39	150.50±3.56	42.42±3.45	272.47±0.70	0.60±0.05	1.88	2.24	0.00	1.35
5664	44.05	665	4.24±0.15	1320.92±1.20	1594.78±2.18	153.48±3.72	44.99±0.99	273.87±2.05	0.68±0.03	1.46	1.36	0.00	1.38

4.2. Maturation characteristics indicated from laser Raman spectroscopy

The degree of condensation and structural order of sedimentary organic matter in source rock increases with the increasing degree of thermal evolution. The first-order vibration peak parameters of laser Raman spectroscopy reflect the lattice structure, chemical bond synthesis, and fracture of carbon materials. Laser Raman spectroscopy of kerogen have two main peaks, namely G band and D band. Some scholars have analyzed the correlation between the laser Raman maturity parameters and the measured maturity of shale organic matter. The difference between the G and D Raman peak positions is the optimum parameter to evaluate the maturity of shale with a Ro range of about 0.50-3.50% (Henry et al., 2019; Sauerer et al., 2017; Zhou et al., 2014).

12 typical samples of the Shahezi with different maturities were selected. To obtain stable parameters, the baseline was corrected to be linear, and the Lorentzian function was used to fit the D and G Raman peaks without further decomposition. The D Raman peak (disordered peak) reflects the structural defects of vibration of heteroatoms, carbon lattice and the vacancy of aromatic ring lamellae. The Raman shift is in the range of 1250-1450 cm^{-1}(Henry et al., 2019; Hou et al., 2019; Sauerer et al., 2017). G Raman peak (ordered peak) reflects the tangential stretching vibration of the C = C bond; the Raman shift is in the range of 1500-1650 cm^{-1} (Wang and Li, 2016). The parameters of the laser Raman spectra calculated in this study include the position of G and D bands (W_D and W_G), peak position difference (RBS = $W_G - W_D$), full width at half maximum (FWHM) for the G and D peaks, and the integrated intensity ratio (I_D/I_G) (where I represent the peak height).

In the laser Raman spectra of the whole-rock shale samples, the minerals result in a high fluorescence background (Schopf et al., 2005), however, the high TOC content improves the SNR of the Raman spectra (Sauerer et al., 2017). Previous studies have shown that Raman spectra obtained from fossils and organic matter in rocks of the same geological unit are essentially identical(Schopf et al., 2005). These spectra are very similar to the Raman spectra of kerogen isolated from the corresponding formation

rocks. The mineral-organic aggregation (MOA) in rock contains only a very small amount of organic matter, while the solid pitch is basically a pure organic matter. The laser Raman spectra of the two were basically the same, which showed that the laser Raman technique is highly sensitive to the carbonaceous matter in high maturity rocks(Xiao et al., 2020). Figure 5 shows the enhanced uncertainties of the laser Raman spectroscopy parameters (FWHM and RBS) for samples with 2%Ro (TOC=1.31%) and 3%Ro (TOC=0.97%) respectively. Lower TOC content may be part of the reason for this phenomenon. This is in general agreement with Xiao et al. (2020) who showed that large fluctuations in sample data are mainly attributable to the low TOC content in the MOA. We observed very strong uncertainties in the W_D and RBS data for two samples with Ro of 1.89 % and 1.96 %, which are likely to be caused by the difficulty in identifying the D peaks in the un-deconvolved spectrum of the two samples. The relationship between the maturity and the laser Raman spectra parameters are shown in Fig 4. As the sample's maturity increases, the peak position difference between the D and G Raman peaks and the sharpness of the peaks increase. When the maturity exceeds 3.52%, the G Raman peak broadens, and the peak position difference decreases. Previous studies have shown that the high signal intensity between G and D peaks is related to a small band(1500-1550 cm^{-1}), reflecting the sp^2 bonding form of amorphous carbon(Cuesta et al., 1994; Jawhari et al., 1995; Jiang et al., 2019; Sonibare et al., 2010). Therefore, in the process of Ro increasing to 3.52 %, the increase of RBS may be due to the decrease in the number of amorphous structures in the compound. When entering a higher maturity stage (Ro > 3.52 %), the decrease of RBS may be related to the increase of aromaticity. During aromatic materials coalesce into larger clusters, a few of the aliphatic side chains between the aromatic rings(i.e. C-C on hydroaromatic rings、C-H on aromatic rings、Caromatic-Calkyl and aromatic (aliphatic) ethers)will fall off(Baysal et al., 2016; Guedes et al., 2010; Lünsdorf, 2016; Negri et al., 2002; Sadezky et al., 2005; Zhang and Li, 2019). The lowest FWHM of the G band in this study is 38.7 cm^{-1}, which is much larger than the reported size of pyrolytic graphite and carbon nanotubes (Hiura et al., 1993; Kastner et al., 1994; Sonibare et al., 2010). This feature

of FWHM indicates that the carbon crystallinity in the samples in this study is low. With the increase of maturity, G and D bands gradually become sharp and narrow, especially the sharp decline trend between FWHM and Ro of D band after the 'turning point' and the appearance of crystalline graphite, indicating that the orderliness of kerogen structure in the thermal evolution process gradually increases.

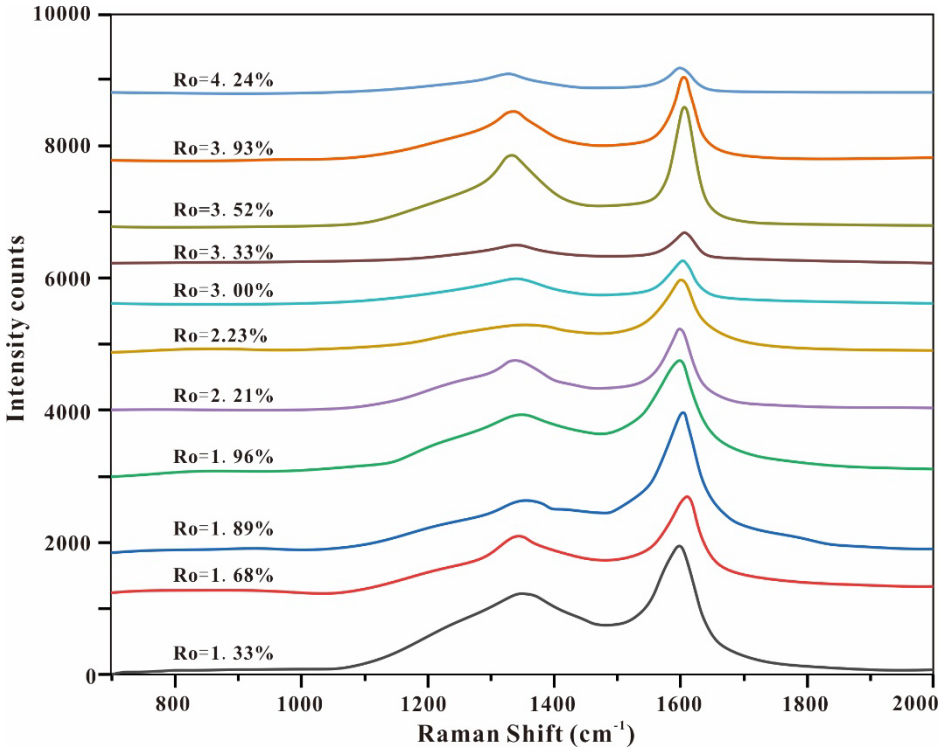

Fig. 4 Laser Raman spectra of samples with different maturities (the spectra have all been offset vertically for clarity and all spectra have the same intensity scale)

The half-peak widths of the D and G peaks show a good inverse correlation with organic matter maturity, as the sample maturity increases, the half-peak widths of the D and G peaks decrease. The average half-peak width of the D (G) peak decreases from 220 cm^{-1} (78 cm^{-1}) at Ro of 1.33% to 150 cm^{-1} (42 cm^{-1}) at Ro of 3.52%. It is worth noting that when Ro is in the range of 3.52%-3.93%, the half-peak widths of the D and G Raman peaks decrease sharply and then increase gradually. The width of D and G peaks is mainly determined by the degree of structural defects and crystallite size of carbon(Kouketsu et al., 2014; Pasteris and Wopenka, 1991; Yui et al., 1996; Zhang and Li, 2019). Moreover, the G peak is the Raman active vibration attributing to crystalline graphite and mainly results from the breathing of aromatic rings in the graphene

sheets(Li et al., 2006; Pasteris and Wopenka, 1991; Pimenta et al., 2007; Reich and Thomsen, 2004; Tuinstra and Koenig, 1970). When Ro is less than 3.33 % -3.52 %, the crystallite size of carbon in kerogen increases continuously, and the G and D peaks are gradually sharp in Raman spectra. When Ro is between 3.33 % and 3.52 %, the FWHM of peak D decreases sharply, and the decrease trend of FWHM of peak G slows down and then increases reversely, which can be explained as the amorphous carbon in kerogen begins to transform into crystalline graphite (Kouketsu et al.， 2014). Previous studies have shown that this 'turning point' represents a significant change in the vibrational modes of carbon molecules in organic matter(Liu et al., 2013; Wang et al., 2015). In the process of coalification, there may also be four to five chemical structural mutations, resulting in a series of changes in the optical and chemical properties of coal. (Carr and Williamson, 1990; Li, 2007; Liu et al., 2013; Lünsdorf, 2016; Schito et al., 2017; Taylor et al., 1998). Some scholars believe that the mutation of kerogen's chemical structure at Ro = 3.5 % can be compared with the fifth coalification mutation in metamorphic anthracite. The chemical structure jump is considered to represent the discontinuity of the nature of kerogen in the thermal evolution process, which is characterized by the termination of most amorphous carbon conversion and the sharp increase of aromatic conjugation with the increase of thermal maturity(Hou et al., 2019). The changes in the peak positions of the D and G peaks during the thermal evolution exhibit regularity. As the maturity increases and Ro is in the range of 1.33-3.52%, the Raman shift of the D peak shows a decreasing trend, this is considered to be related to the progressive growth of linear aromatic structures. A variety of chemical reactions occurred in this stage, which changed the molecular structure and chemical composition of polycyclic aromatic hydrocarbons with different sizes, decomposed aliphatic compounds, condensed aromatic rings, and then cured. (Lünsdorf, 2016), and that of the G peak shows an increasing trend. When the maturity is 3.52-3.93%, the Raman shift of the D peak shows an increasing trend. At this time, the number of free radicals reaches the maximum, which is conducive to the recombination of aromatic units. Since then, many properties of polycyclic aromatic hydrocarbons with different sizes have

changed rapidly, especially aromaticity, size of aromatic clusters, cyclization and reflectance(Taylor et al., 1998). The size of aromatic compounds increases gradually, and that of the G peak decreases significantly (Fig 5), which is consistent with the sudden broadening of the G peak at this maturity. The RBS increases from 242 cm^{-1} to 272 cm^{-1} as Ro increases from 1.33% to 3.52%, followed by a small decrease. I_D / I_G represents, to some extent, the extent of aromatic growth(Du et al., 2014; Guedes et al., 2010; Zhang and Li, 2019; Zhou et al., 2014). When Ro < 2.23 %, the I_D / I_G value decreased slightly. When Ro was between 2.23 % and 3.52%, the increase of I_D / I_G value might be related to the slow growth of aromatic rings. At this stage, the structure of aromatic ring remained relatively stable, and amorphous carbon gradually decreased. When Ro > 3.52%, I_D/I_G increases rapidly from 0.54 to 0.67, showing a significant positive correlation with Ro. The sharp increase in I_D / I_G may mean the rapid growth of aromatic clusters. The evolution of laser Raman parameters is comparable to those in previous studies (Wang et al., 2015; Xiao et al., 2020). Most of the parameters used in the analysis have inflection points or show inversions when Ro is 3.52-3.93%. This phenomenon has also been reported in other studies (Henry et al., 2019; Lünsdorf, 2016; Quirico et al., 2005; Schopf et al., 2005; Xiao et al., 2020). Some scholars believe that this inflection point in the laser Raman spectrum represents the transformation of organic matter from amorphous carbon to crystalline graphite, which is consistent with the fact that the order degree of the carbon layer structure of shale organic matter increases with the degree of thermal evolution (Hou et al., 2019).

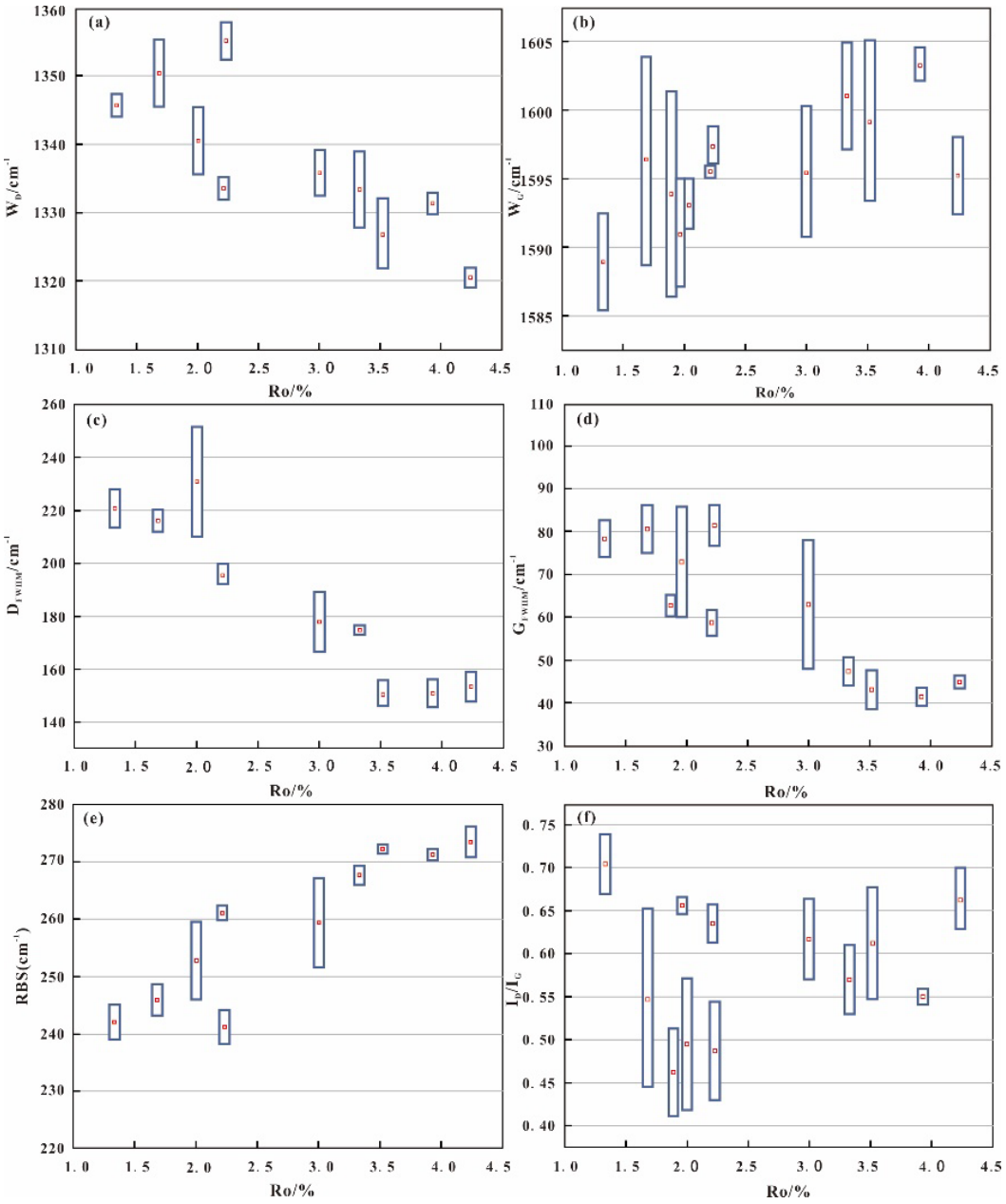

Fig. 5. Relationship between laser Raman parameters and vitrinite reflectance of organic matter in the Shahezi formation (the box represents the range of the measured Raman parameters, and the midpoint in the box indicates the average)

4.3 Maturation characteristics indicated from FT-ICR MS

4.3.1 Elemental and compound classes from FT-ICR MS

The results of the APPI (+) FT-ICR MS (Fig. 6) show a very complex composition of compounds in the hydrocarbon source rock samples of the Shahezi formation in the

Songliao basin, Horsfield et al (2022) analyzed Fourier transform ion cyclotron resonance mass spectrometry (FT-ICR MS) data from SK-2 well with a special focus on molecular H_2 generation, and focused on aromatization and cracking reactions of organic matter during thermal evolution. The extracts include hydrocarbons (HC) and non-hydrocarbon compounds. Formula assignment was performed using the elemental isotopes ^{1}H, ^{12}C, ^{13}C, ^{14}N, ^{16}O, and ^{32}S, with the upper thresholds $N \leq 2$, $O \leq 6$, and $S \leq 2$; C and H were unlimited. If no chemical formula could be assigned within the allowed mass error of 1 ppm, the data were excluded. The elemental composition of each target compound is CcHhNnOoSs. Double-bond equivalents (DBEs), which are defined as the number of double bonds and rings, were calculated for each elemental composition using the equation $DBE = c - (h/2) + (n/2) + 1$(correspond to CcHhNnOoSs). According to the number of N, O, and S heteroatoms in the molecule, the non-hydrocarbon compounds were categorized in six classes: Ox, Ny, OxNy, Sz, OxSz, and NySz.

The aromatic HC species

APPI ionizes non-polar hydrocarbons and is used to detect aromatic HC compounds (Walters et al., 2011). FT-ICR MS (Fig. 6a) shows that in extracts of source rocks with relatively low maturity (Tmax range from 510 °C to 597 °C) HC compounds account for the largest proportion of all compound classes, and the total monoisotopic ion abundance (TMIA) is 23.17%-63.65%. The TMIA of the samples exceeds 50%, except for the samples obtained at a depth of 3866 m (Tmax = 579 °C). The HC compounds can be divided into three groups: DBE1-5, DBE6-15, and DBE15 +, corresponding to low, medium, and high DBE groups representing compounds with an increasing molecular size of the aromatic core structure (Han et al., 2022b). As the maturity increases, there is likely a strong decrease in signals, the consumption of HC in the polar molecular compounds of the shale organic matter decreases sharply due to pyrobitumen formation(Mahlstedt et al., 2022), and the TMIA is 0.97%-6.79%. Fig 7 shows that the TMIA, DBE, and carbon number of the HC change with maturity. When the maturity is relatively low, the range of the DBE and carbon number is wider, and

the compounds show higher aromaticity and larger molecular size (larger ring system).

Ox species

Ox compounds are the main components of nonhydrocarbon compounds. The Ox species mainly consist of O_1, O_2, and O_4 compounds in all extracts (Fig. 6.b). The TMIA ranges from 0% to 16.96%. The O_1 compounds detected in the APPI (+) mode are presumed to be aliphatic and aromatic aldehydes, alcohols, ketones, and furans (Huba et al., 2016). The DBE and carbon numbers of the O_1 compounds are similar to those of the HC compounds (Fig. 7). The difference in the TMIA between different source rock O_1 compounds is small (5.25%-15.15%), and the TMIA is 7%-10%. Conversely, the content of the O_{2-6} compounds in different source rock increases with an increase in maturity.

Ny and NyOx species

The Ny compounds in the samples are predominantly N_1, and the TMIA range of N_1 is 0.15% to 17.76%. The N_1 compound shows similar distribution characteristics to the CH compound, i.e., the abundance decreases sharply as maturity increases. All Ny compounds increase and then decrease with increasing maturity (Fig 6c). In source rock with relatively low maturity (Tmax in the range of 510 °C to 597 °C), the content of the Ny compounds is relatively high, with TMIA ranges of 4.45% to 17.76% for the N_1 compounds and from 0.07% to 1.34% for the N_2 compounds. When the maturity is high (Tmax of 618 °C-665 °C), the Ny compound content is relatively low, with TMIA ranges of 0.15% to 3.79% for the N_1 compounds and from 0% to 0.08% for the N_2 compounds.

The contents of NyOx ($N_{1-2}O_{1-2}$ compounds) in the extracts vary substantially, including $N_1O_1/N_1O_2/N_2O_1/N_2O_2$ (Fig 6e). The N_1O_1 compounds are N_1 compounds with hydroxyl groups, and the N_1O_2 compounds are N_1 compounds with carboxyl groups (Jiang et al., 2021). The N_1O_1 compounds dominate the NyOx analogs with a TMIA range of 4.64% to 30.44%. In contrast to the Ny analogs, the TMIA of the NyOx analogs is relatively low in the low mature stage and suddenly increases in the high mature stage. For example, when N_1O_1 is at 510 °C-597 °C, the TMIA range is 4.64% to 10.44%, and when Tmax = 597 °C, the TMIA increases to 30.44%. The TMIA of the

N_1O_2, N_2O_1, and N_2O_2 compounds in the source rock at low maturity is extremely low (< 4.85%). In contrast, at relatively high maturity (Tmax between 630 °C and 665 °C), the TMIA of the N_1O_2, N_2O_1, and N_2O_2 compounds is higher, with ranges of 0.51%-6.37%, 0.22%-8.25%, and 1.52%-9.87%, respectively. As the maturity increases, nitrogen-containing compounds with long carbon chains and low unsaturation levels in organic matter become unstable, and basic nitrogen compounds with more fused rings occur in organic matter.

Sulfur-containing species

The APPI (+) method is sensitive for the ionization of organosulfur compounds in organic matter. Sulfur-containing species include Sz, SzOx, and NySz. The TMIA of Sz is the highest, ranging from 0.64% to 10.32%. There are significant differences in the TMIA of the Sz compounds for different maturation stages (Fig 6d), indicating that the HC, N_1, and Sz compounds in organic polar molecules decompose or transform in large quantities during the evolution of Tmax from 597 °C to 618 °C. As a result, there is a sharp decrease in the content, and the range of the DBE and the carbon number of the S_1 compounds becomes narrower (Fig 7). The S_1 compounds with DBE ≥ 3 are most likely to be aromatic compounds containing thiophene units. It is speculated that S_1 compounds with a lower DBE number are alkyl thiolanes (tetrahydrothiophenes) or alkyl thianes (tetrahydrothiopyrans) (Liu et al., 2018).

The TMIA of the SzOx and NySz compounds is generally low, not exceeding 2.94% (Fig 6.f, g). At the relatively low maturity stage (Tmax < 630 °C), S_1O_1 compounds are the major fraction of SzOx, with the TMIA generally ranging from 0.5% to 1%, and S_1O_2/S_1O_3/S_1O_4 are absent. At relatively high maturity (Tmax＞630 °C), the abundance of S_1O_2/S_1O_3/S_1O_4 increases with the reaction time of the Sz compounds, indicating that Sz and Ox are combined. The content of the NySz compounds varies substantially, and the sample with a Tmax of 630 °C has an unusually high content of NySz compounds with TMIA=2.69%.

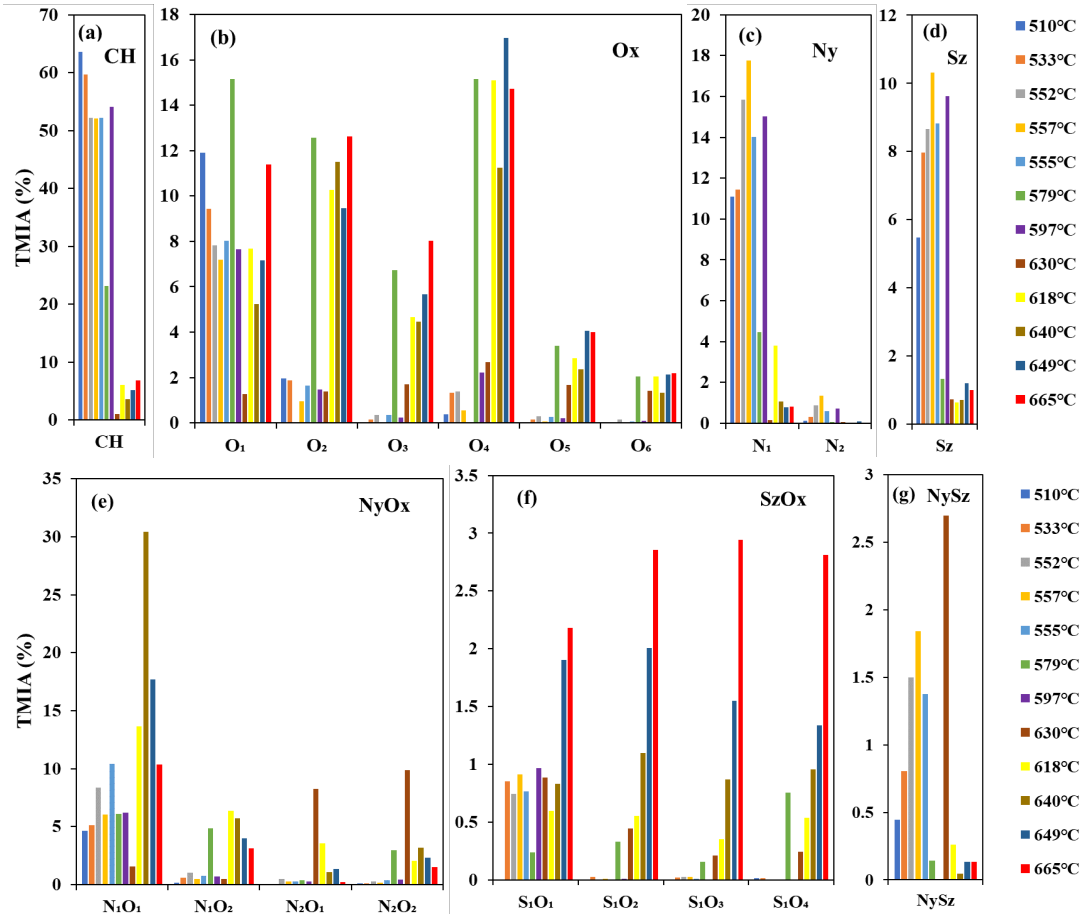

Fig 6. The relative contents of organic molecular compounds with different maturities. Ox: elemental class containing only oxygen as heteroatom, Ny: elemental class containing only nitrogen as heteroatom, Sz: elemental class containing only sulfur as heteroatom, NySz: elemental class containing a combination of nitrogen and sulfur as heteroatoms, the same applies for the OxNy and OxSz classes, HC: elemental class comprised of pure hydrocarbons. Within the compound classes the number of heteroatoms is specified (e.g., in the O_1 class each molecule contains one oxygen atom as heteroatom and so on).

In Fig 6, the TMIA of the HC, N_1, O_1, and S_1 compounds decrease with an increase in maturity. A similar trend is observed in the TMIA plot of the DBE *vs*. the carbon number of those species. Fig 7 shows the relative ion abundance (TMIA) plots of the DBE *vs*. the carbon number of the four compound classes for different mature source rock obtained from the APPI (+) FT-ICR MS. In the sample with a depth of 3376 m (Tmax = 510 °C), the N_1 compounds have a DBE range of 13-39 and a carbon number range of 17–58, and the compounds are abundant. The compounds containing 12, 15,

and 18 DBE are primarily alkyl carbazole compounds with 1-3 benzene rings (Zhu et al., 2011). However, in the sample with a depth of 5664 m (Tmax = 665 °C), the DBE and carbon number of the N_1 compounds are variable, and all alkylcarbazole compounds have been consumed. The results indicate that maturity is the factor causing the difference of organic matter composition in different source rocks. The polar molecular compounds of organic matter in high-mature source rock are mainly high DBE compounds with a wide range of carbon numbers. The polar molecular compounds of organic matter in overmature source rock are predominantly low DBE compounds, and the range of the carbon number is also narrower.

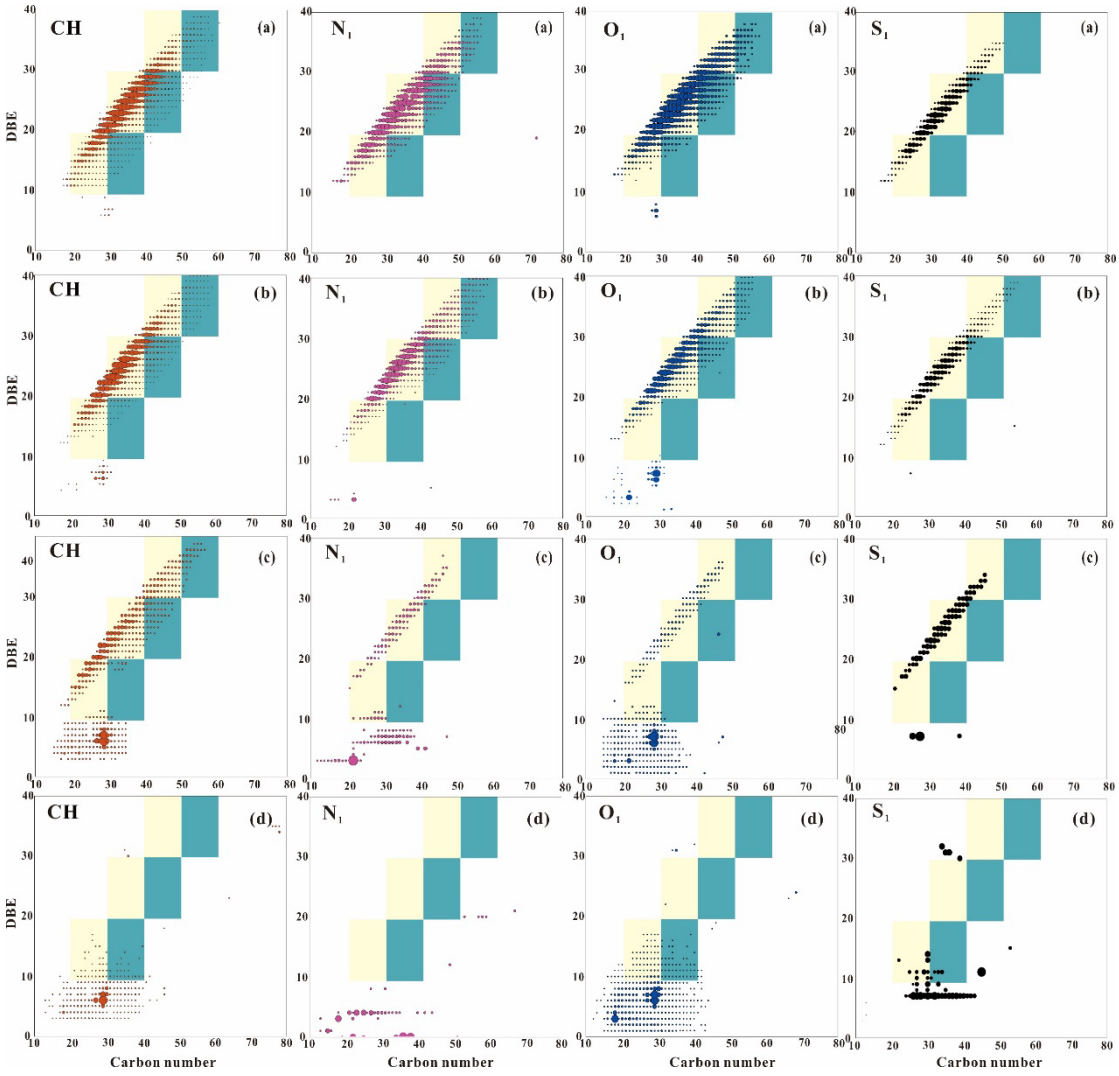

Fig.7. Relative ion abundance (TMIA) of DBE *vs*. the carbon number for four species of organic matter with different maturities. Yellow areas are indicative of lower carbon numbers associated with higher maturities, whereas green areas indicate higher carbon numbers and lower maturities. The depth of (a) is 3376 m, Tmax=510 °C, the

depth of (b) is 3676 m, Tmax=579 °C, the depth of (c) is 4426 m, Tmax=597 °C, and the depth of (d) is 5664 m, Tmax=665 °C

4.3.2 Maturity index of FT-ICR MS

An earlier study of Noah et al. (2020a) revealed progressive changes in DBE *vs* carbon number which could be used to establish a new maturity parameter with strong linearity up to 2% Ro. In this study we extended the calculation method of Noah et al. (2020a) to analyze the structure and variation characteristics of unsaturation of samples (0.59 % <Ro <4.24 %). The long-chain and short-chain compounds were distinguished by the X-axis carbon atom number, with a range of 10-70. The compound's unsaturation was distinguished by the Y-axis DBE with a range of 10-40. It is generally believed that the number of aromatic structures increases with an increase in thermal maturity of organic matter, whereas the number of aliphatic structure decreases, and the hydrogen-carbon ratio decreases (Hunt, 1995; Noah et al., 2020a; Poetz et al., 2014; Welte and Tissot, 1984). It is concluded that DA1 contains compounds with higher degrees of polymerization and aromatization, and DA2 contains compounds with lower degrees of polymerization and higher degrees of alkylation. Based on this assumption, the signal abundances of DA1 and DA2 are determined. The MAT (Maturity index of FT-ICR MS) was calculated using the equation MAT = (the signal abundances of DA1)/ (the signal abundances of DA2). Theoretically, MAT reflects the ratio of low-carbon number to high-carbon number compounds and the degree of lipidation of the compounds. The larger the MAT value, the higher the maturity of the compound is.

Eleven marine shale samples with relatively favorable geochemical parameters (Ro ranging from 0.59% to 4.07%) were selected from the lower Arthur Creek strata of the middle Cambrian in the southwestern Georgina basin (Noah et al., 2020b). The MAT parameters were compared to evaluate the applicability of the MAT index to assess shales with low maturity and from different sedimentary environments. The data set expands the range of maturity evaluated by the MAT parameters to the low to overmature stage.

The Tmax values of the two groups of samples were fitted and compared with the MAT values. The fitting results show that the Tmax has a high positive correlation with the MAT values for each compound at Tmax values of 420 °C to 600 °C. The coefficient of determination (R^2) ranges from 0.90 to 0.96 (Fig. 8). The fitted line of the S_1 compounds has a large slope, and the values are dispersed; the standard error (Se) is 1.38. This can be explained by the distribution of S_1 compounds in DBE and carbon Fig. Only a small number of compounds fall in the green region, indicating that when Tmax is 420 °C to 600 °C, the part of low carbon number in sulfur compounds dominates (Fig. 7). In contrast, the fitting results of the CH, O_1, and N_1 compounds show less dispersion, with an Se of 0.38 to 0.56. The fitting results of the four compounds of the Shahezi source rock and Arthur Creek shale are the best at Tmax values of 420 °C to 600 °C.

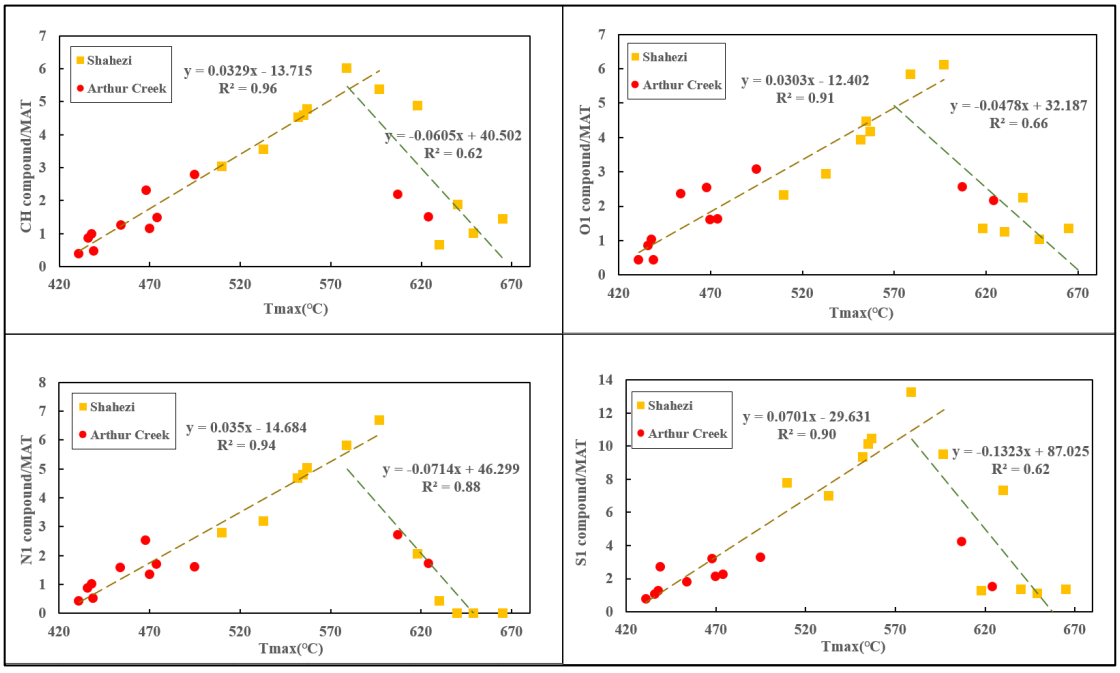

Fig. 8 MAT *vs* Tmax of HC, O_1, N_1, and S_1 compounds. Data points for the upward trend line are from 9 Arthur Creek formation samples and 7 Shahezi formation samples at 431°C <Tmax<597°C; Data points for the downward trend line are from 7 Shahezi formation samples and 2 Arthur Creek formation samples at 579°C <Tmax<665°C.

When Tmax is in the range of 600 ° C to 670 ° C (corresponding to matagenesis),

the correlation between MAT and maturity of four typical compounds is reversed. The correlation coefficients between MAT parameters of different compounds and Tmax are quite different, which may be related to the types and quantities of compounds in soluble organic matter that can be extracted from the samples at the over-mature stage. For example, the signal intensity of N_1 compound calculated by MAT formula in Fig. 7d basically disappears, while some signal intensities of the other three compounds are still distributed in the computable region. The N_1 compounds have the highest and most significant negative correlation between MAT and Tmax (R^2 = 0.88). The N_1 compounds of Shahezi source rock and Arthur Creek shale showed strong continuity in the Tmax-MAT fitting results. The MAT parameters of the two different types of source rocks have similar inversion phenomena in the high-to-mature stage, which reveals the variation characteristics of compound components in the soluble organic matter of source rock in the high-to-mature stage to some extent. In the high thermal evolution stage, condensed high DBE aromatics are directly integrated into pyrobitumen that cannot be detected by FT-ICR MS with the condensation reaction of polycyclic aromatic hydrocarbons (Horsfield et al., 2022). The MAT values of CH, O_1 and S_1 compounds also showed negative correlation with the corresponding Tmax, and their R^2 is between 0.62 and 0.66.

5 Implications

During the thermal evolution of organic matter, the condensation and aromatization reactions often proceed synchronously, resulting in the formation of high-carbon compounds with strong thermal stability. During this process, the composition of organic matter compounds changes, i.e., as the maturity increases, the functional groups and side chains around the aromatic ring in the molecular structure break off, and the number of aromatic structure increases while the number of aliphatic structure decreases (Schenk et al., 1986; Seifert and Moldowan, 1978). In the source rocks of this study, the increasing degree of polymerization of soluble bitumen, insoluble kerogen and pyrobitumen is observable in laser Raman spectroscopy and FT-ICR MS.

The two maturity evaluation methods both reflect that whether soluble or insoluble kerogen and pyrobitumen in Shahezi formation, when the maturity reaches a certain stage, the molecular structure and composition of the compound will change abruptly. The turning point of molecular structure of soluble organic matter and insoluble organic matter is different (Fig. 9).

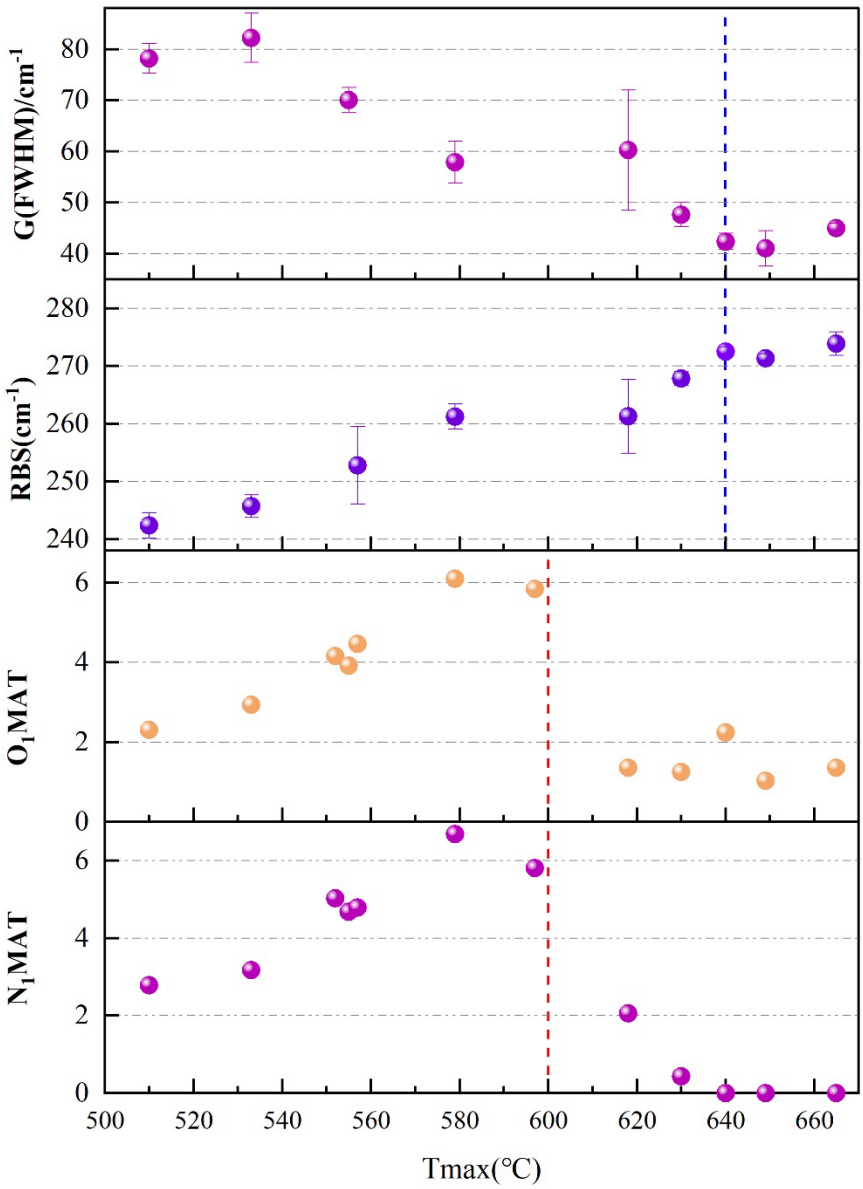

Fig. 9 Comparison of Tmax, MAT and laser Raman spectroscopy parameters. Error bars represent one standard deviation.

In Raman spectra, with the increase of thermal evolution degree, when Ro <

3.33%-3.52%, the crystallite size of carbon in kerogen increases, the number of amorphous structure decreases, and the linear aromatic junction shows a gradual growth trend (Lünsdorf, 2016). At this time, the peak position difference between the D and G Raman peaks and the sharpness of the peaks increase, the half-peak widths of the D and G peaks decrease. When Ro>3.33%-3.52%, the transformation of most amorphous carbon in kerogen was terminated, the aromatic units of heteroatomic compounds were recombined, and the size of aromatic compounds gradually increased(Kouketsu et al., 2014). The degree of aromatic conjugation and the degree of carbon crystallization increased sharply with the increase of thermal maturity, and amorphous carbon began to transform into crystalline graphite(Hou et al., 2019). The Raman shift of the D peak shows an increasing trend, I_D / I_G increases sharply. The half-peak widths of the D and G Raman peaks decreased sharply and then increased gradually.

The results showed that MAT was positively correlated with maturity for Ro values of 1.33%-2.5% and Tmax values of 420 °C-600 °C. The MAT decreased as the Ro exceeded 2.5% and Tmax exceeded 600 °C. Polar molecular compounds in the calculation area of MAT (DBE in the range of 10-40 and carbon numbers in the range of 20-60) were not observed in some samples. This phenomenon is not a coincidence but is related to the overmature samples of the Arthur Creek formation in the Georgina basin, Australia, and the Shahezi formation in the Songliao basin. In the DBE-carbon number cross-plot, the DBE and carbon number decreased with an increase in the thermal maturity of organic matter. The decrease was more pronounced at the interface between high maturity and over maturity. Therefore, the decrease in the MAT may be related to the thermal stability of organic compounds and the formation of pyrobitumen and graphite. The chemical bonding of organic molecules is y based on covalent bonds; the bond length and bond energy of covalent bonds jointly determine the thermal stability of molecular compounds. The thermal evolution of organic matter is accompanied by the detachment of side chains and the occurrence of polycondensation reactions (Poetz et al., 2014). Macromolecular compounds with a shorter bond length and higher bond energy are generated, but these macromolecular compounds also have

thermal stability limits. When the pyrolysis temperature and time reach the limit, the macromolecule compounds may suddenly collapse, leading to a sharp decrease in the relative content of high DBE and high carbon number compounds, which may be accompanied by the generation of methane (Lorant and Behar, 2002). During thermal evolution, organic matter is continuously cracked, non-carbon elements are discharged in the form of volatiles, and the H/C atomic ratio continues to decline. In the overmature stage, the further condensation of organic matter leads to the formation of carbonaceous residues with a lower hydrogen content, namely pyrobitumen and graphite(Hou et al., 2019). These high DBE and high carbon number products cannot be extracted and cannot be analyzed by FT-ICR MS.

The decrease in the MAT means that the parameter characteristics of some overmature samples in Shahezi formation are similar to those of samples with relatively low maturity. As a result, the application scope of MAT is limited, and its accuracy may be low if the MAT results are not compared with other maturity indices. Horsfield et al (2022) had normalized the APPI (+) intensity of the samples with different maturities and subtracted the results of the lower maturity samples from those of the higher maturity samples in the DBE-carbon number cross-plot to determine the formation and loss of target compounds during the thermal evolution of organic matter. The DBE of compounds with a given carbon number increases with an increase in maturity. The carbon number in the compounds with a given DBE decreases significantly with an increase in maturity. Therefore, aromatization may not be the dominant process. It is also noteworthy that the newly formed high-DBE aromatics may be part of the pyrobitumen rather than being reflected in the DBE-carbon cross-plot. During the thermal evolution, some compounds are not transformed into new compounds and are not decomposed or polymerized. Their signal intensity changes only with the formation of other types of new compounds. Therefore, this subtraction may lead to a net loss in the abundance of all compounds. This attempt explains the change characteristics of compounds during thermal evolution using the DBE-carbon cross-plot. To some extent, it explains why the MAT decrease.

Laser Raman spectroscopy and FT-ICR MS have different focuses in evaluating the maturity of organic matter. The in-plane E_{2g2} vibrational mode (A vibrational mode causing a single strong first order line at 1582 cm^{-1}) of carbon atom in the aromatic ring structure (sp^2 carbon) shows D_{6h}^4 symmetry, and Raman-active A_{1g} (the Raman active modes formed by large molecules with different sizes and shapes) symmetry associated with lattice defects and discontinuities of the sp^2 carbon network(Tuinstra and Koenig, 1970). These characteristics will have corresponding characteristic peaks in the Raman spectra. By analyzing the parameters of characteristic peaks in the Raman spectra of different solid organic matter, the structure and evolution path characteristics of aromatic moieties in solid organic matter at different maturity stages can be obtained. The elemental contents of carbon, hydrogen, oxygen, nitrogen, and sulfur in the organic matter of hydrocarbon source rocks were investigated using high-precision and high-resolution FT-ICR MS. The molecular composition and relative content were analyzed by a normalization algorithm, and the CH, O_1, N_1, and S_1 compounds were used as targets. The CH compounds represent aromatic components, and the O_1 compounds represent various oxygen-containing compounds with different types of oxygen bonds, such as aldehydes, alcohols, ketones, furans, and carboxylic acids bonded with aromatic nuclei. The N_1 compounds represent various pyridine and pyrrole compounds, and the S_1 compounds are most likely represent aromatic thiophenes(Noah et al., 2020a). The dynamic changes in the relative content of the organic matter molecular compounds were described by the carbon number and DBE diagram. Finally, signal intensity conversion of each compound was performed to quantify the maturity level of organic matter. The MAT was significantly and highly correlated with the Ro and Tmax, indicating its applicability to maturity evaluation of Shahezi formation. The two methods can well complement each other in the evaluation of organic matter maturity. Since tar pitch and graphite with high DBE and high carbon number are difficult to be extracted, the MAT values of some over-mature samples are similar to those of samples with relatively low maturity. Combined with the characteristic peak parameters of laser Raman spectroscopy of samples with different maturity, the samples with over-mature

and low maturity can be effectively distinguished. MAT can accurately and continuously reflect the maturity change change trend of characteristic compound in soluble organic matter and the dynamic change law of relative content of compound molecules. Combined with the chemical structure change characteristics of aromatic moieties in solid organic matter reflected by laser Raman spectroscopy, the two methods can reveal the structural characteristics of organic matter molecules in thermal evolution stage from different angles, which is of great significance to the maturity study of deep source rocks in petroliferous basins.

6 Conclusion

The organic matter of the deep Shahezi source rock in the Songliao basin has good hydrocarbon potential. The results of various maturity evaluation methods showed that the deep source rock Ro of Shahezi formation was greater than 1.3%, Tmax exceeded 500 °C, and the thermal evolution degree of organic matter was high to overmature. Most of the parameters of laser Raman spectroscopy in Shahezi formation samples showed an inflection point or reversal in the Ro range of 3.52-3.93%, indicating that the structural order and of aromaticity organic matter increased as maturity increased.

The comparison of the Ro, Tmax, and MAT indices showed that MAT of samples was positively correlated with maturity at Ro values of 1.33%-2.5% and Tmax values of 420 °C-600 °C. Unlike the S_1 compound, the fitting results of the CH, O_1, and N_1 compounds were strongly correlated with the sample's maturity(R^2>0.9) and exhibited weak dispersion (Se<0.56). As the Ro exceeded 2.5% and Tmax exceeded 600 °C, the MAT showed a decreasing trend. . It is thought that the decrease in the MAT may be related to the thermal stability of organic matter molecular compounds and the generation of bitumen and graphite.

The MAT index quantified the structural characteristics of target molecular compounds during the thermal evolution of organic matter using the "element-molecule-compound" analogy. It enabled the numerical evaluation of organic matter maturity and had good application prospects effect. At the same time, laser Raman

spectroscopy can well reveal the structural characteristics of aromatic moieties in thermal evolution process. The two methods complement each other, confirmed similar growth of aromatic rings take place, provided insights into the characterization of the molecular structure evolution pattern of high-over mature organic matter, and will provide key parameters for deep unconventional oil and gas genesis and resource exploration.

Acknowledgments

This research was supported by the National Natural Science Foundation of China (Grant No. 42072168), the National Key R&D Program of China (Grant No. 2019YFC0605405) and the Fundamental Research Funds for the Central Universities (Grant No. 2022YQDC06). The editors and anonymous reviewers are gratefully acknowledged.

Reference

ASTM, 2011. D2797 Standard practice for preparing coal samples for microscopical analysis by reflected light. ASTM International West Conshohocken, PA.

Barker, C., 1974. Pyrolysis techniques for source-rock evaluation. AAPG Bulletin. 58, 2349-2361.

Baysal, Mustafa, Yurum, Alp, Yildiz, Burcin, Yuda, 2016. Structure of some western Anatolia coals investigated by FTIR, Raman, C-13 solid state NMR spectroscopy and X-ray diffraction. International Journal of Coal Geology. 163, 166-176.

Bernard, S., Horsfield, B., Schulz, H.M., Wirth, R., Schreiber, A., Sherwood, N., 2012. Geochemical evolution of organic-rich shales with increasing maturity: A STXM and TEM study of the Posidonia Shale (Lower Toarcian, northern Germany). Marine and Petroleum Geology. 31, 0-89.

Bertrand, R., Malo, M., 2001. Source rock analysis, thermal maturation and hydrocarbon generation in the Siluro-Devonian rocks of the Gaspe Belt basin, Canada. Bulletin of Canadian Petroleum Geology. 49, 238-261.

Beyssac, O., Goffé, B., Petitet, J.-P., Froigneux, E., Moreau, M., Rouzaud, J.-N., 2003. On the characterization of disordered and heterogeneous carbonaceous materials by Raman spectroscopy. Spectrochimica Acta Part A: Molecular and Biomolecular Spectroscopy. 59, 2267-2276.

Birdwell, J.E., Jubb, A.M., Hackley, P.C., Hatcherian, J.J., 2021. Compositional evolution of organic matter in Boquillas Shale across a thermal gradient at the single particle level. International Journal of Coal Geology. 248.

Boreham, C.J., Crick, I.H., Powell, T.G., 1988. Alternative calibration of the Methylphenanthrene Index against vitrinite reflectance: Application to maturity measurements on oils and sediments. Organic Geochemistry. 12, 289-294.
Burgess, J.D., 1977. Historical review and methods of determining thermal alteration of organic materials. Palynology. 1, 1-7.
Carr, A., Williamson, J., 1990. The relationship between aromaticity, vitrinite reflectance and maceral composition of coals: implications for the use of vitrinite reflectance as a maturation parameter. Organic Geochemistry. 16, 313-323.
Chen, J., Wang, D., Zhang, X., Li, C., 2000. Analysis of volcanic facies and apparatus of Yingcheng Formation in Xujaweizi Faulting Depression Songliao Basin Northeast China. Earth Science Frontiers. 7, 371-379.
Court, R.W., Sephton, M.A., Parnell, J., Gilmour, I., 2007. Raman spectroscopy of irradiated organic matter. Geochimica Et Cosmochimica Acta. 71, 2547-2568.
Cuesta, A., Dhamelincourt, P., Laureyns, J., Martínez-Alonso, A., Tascón, J., 1994. Raman microprobe studies on carbon materials. Carbon. 32, 1523-1532.
Cui, J., Zhu, R., Wang, C., Gao, Y., Li, S., Kang, L., 2020. Source/reservoir characteristics and shale gas "sweet spot" interval in Shahezi mudstone of Well SKII in Songliao Basin, NE China. Arabian Journal of Geosciences. 13, 1-13.
Du, J., Geng, A., Liao, Z., Cheng, B., 2014. Potential Raman parameters to assess the thermal evolution of kerogens from different pyrolysis experiments. Journal of Analytical & Applied Pyrolysis. 107, 242–249.
Espitalié, J., Laporte, J.L., Madec, M., Marquis, F., Leplat, P., Paulet, J., Boutefeu, A., 1977. Methode rapid de caracterisation des roches. Mere de leur potential petrolier of de leur degree evolution. Rev. de 1. Inst France Petrol. 32(1), 32-42.
Gai, H., Tian, H., Cheng, P., Zhou, Q., Li, T., Wang, X., Xiao, X., 2019. Influence of retained bitumen in oil-prone shales on the chemical and carbon isotopic compositions of natural gases: Implications from pyrolysis experiments. Marine and Petroleum Geology. 101, 148-161.
Ganz, H., Kalkreuth, W., 1987. Application of infrared spectroscopy to the classification of kerogentypes and the evaluation of source rock and oil shale potentials. Fuel. 66, 708-711.
Gentzis, T., Goodarzi, F., Snowdon, L.R., 1993. Variation of maturity indicators (optical and Rock-Eval) with respect to organic matter type and matrix lithology: an example from Melville Island, Canadian Arctic Archipelago. Marine and Petroleum Geology. 10, 507-513.
Guedes, A., Valentim, B., Prieto, A.C., Rodrigues, S., Noronha, F., 2010. Micro-Raman spectroscopy of collotelinite, fusinite and macrinite. International Journal of Coal Geology. 83, 415-422.
Han, S., Tang, Z., Wang, C., Horsfield, B., Wang, T., Mahlstedt, N., 2022a. Hydrogen-rich gas discovery in continental scientific drilling project of Songliao Basin, Northeast China: new insights into deep Earth exploration. Science Bulletin. 67, 1003-1006.
Han, Y., Noah, M., Lüders, V., Körmös, S., Schubert, F., Poetz, S., Horsfield, B., Mangelsdorf, K., 2022b. Fractionation of hydrocarbons and NSO-compounds during primary oil migration revealed by high resolution mass spectrometry: Insights from oil

trapped in fluid inclusions. International Journal of Coal Geology. 254, 103974.
Hatch, J.R., Daws, T.A., Lubeck, S., Pawlewicz, M.J., Threlkeld, C.N., Vuletich, A.K., 1984. Organic geochemical analyses for 247 organic-rich-rock and 11 oil samples from the Middle Pennsylvanian Cherokee and Marmaton Groups, southeastern Iowa, Missouri, southeastern Kansas, and northeastern Oklahoma. 84-160.
Henry, D.G., Jarvis, I., Gillmore, G., Stephenson, M., 2019. Raman spectroscopy as a tool to determine the thermal maturity of organic matter: Application to sedimentary, metamorphic and structural geology. Earth-Science Reviews. 198, 102936.
Henry, D.G., Jarvis, I., Gillmore, G., Stephenson, M., Emmings, J.F., 2018. Assessing low-maturity organic matter in shales using Raman spectroscopy: Effects of sample preparation and operating procedure. International Journal of Coal Geology. 191, 135-151.
Hinrichs, R., Brown, M.T., Vasconcellos, M.A.Z., Abrashev, M.V., Kalkreuth, W., 2014. Simple procedure for an estimation of the coal rank using micro-Raman spectroscopy. International Journal of Coal Geology. 136, 52-58.
Hiura, H., Ebbesen, T.W., Tanigaki, K., Takahashi, H., 1993. Raman studies of carbon nanotubes. Chemical Physics Letters. 202, 509-512.
Horsfield, B., Clegg, H., Wilkes, H., Santamaría-Orozco, D., 1998. Effect of maturity on carbazole distributions in petroleum systems: new insights from the Sonda de Campeche, Mexico, and Hils Syncline, Germany. Naturwissenschaften. 85, 233-237.
Horsfield, B., Mahlstedt, N., Weniger, P., Misch, D., Vranjes-Wessely, S., Han, S., Wang, C., 2022. Molecular hydrogen from organic sources in the deep Songliao Basin, P.R. China. International Journal of Hydrogen Energy. 47, 16750-16774.
Hou, H., Wang, C., Zhang, J., Ma, F., Fu, W., Wang, P., Huang, Y., Zou, C., Gao, Y., Gao, Y., Zhang, L., Yang, J., Guo, R., 2018. Deep continental scientific drilling engineering in Songliao Basin: Resource discovery and progress in earth science research. Geology in China. 45, 641-657.
Hou, Y., Zhang, K., Wang, F., He, S., Dong, T., Wang, C., Qin, W., Xiao, Y., Tang, B., Yu, R., Du, X., 2019. Structural evolution of organic matter and implications for graphitization in over-mature marine shales, south China. Marine and Petroleum Geology. 109, 304-316.
Huang, D., 1999. Advances in hydrocarbon generation theory (I): Generation and evolution model for immature oils and hydrocarbon. Journal of Petroleum Science & Engineering. 22, 121-130.
Huba, A.K., Huba, K., Gardinali, P.R., 2016. Understanding the atmospheric pressure ionization of petroleum components: The effects of size, structure, and presence of heteroatoms. Science of the Total Environment. 568, 1018-1025.
Hunt, J.M., 1995. Petroleum geochemistry and geology. Petroleum Geochemistry and Geology.
Jarvie, D.M., Hill, R.J., Ruble, T.E., Pollastro, R.M., 2007. Unconventional shale-gas systems: The Mississippian Barnett Shale of north-central Texas as one model for thermogenic shale-gas assessment. Aapg Bulletin. 91, 475-499.
Jawhari, T., Roid, A., Casado, J., 1995. Raman spectroscopic characterization of some commercially available carbon black materials. Carbon. 33, 1561–1565.

Jiang, B., Tian, Y., Zhai, Z., Zhan, Z.-W., Liao, Y., Zou, Y.-R., Peng, P.a., 2021. Characterisation of heteroatomic compounds in free and bound bitumen from different source rocks by ESI FT-ICR MS. Organic Geochemistry. 151, 104147.
Jiang, J., Yang, W., Cheng, Y., Liu, Z., Zhang, Q., Zhao, K., 2019. Molecular structure characterization of middle-high rank coal via XRD, Raman and FTIR spectroscopy: Implications for coalification. Fuel. 239, 559-572.
Kastner, J., Pichler, T., Kuzmany, H., Curran, S., Blau, W., Weldon, D.N., Delamesiere, M., Draper, S., Zandbergen, H., 1994. Resonance Raman and infrared spectroscopy of carbon nanotubes. Chemical Physics Letters. 221, 53-58.
Kouketsu, Y., Mizukami, T., Mori, H., Endo, S., Aoya, M., Hara, H., Nakamura, D., Wallis, S., 2014. A new approach to develop the Raman carbonaceous material geothermometer for low-grade metamorphism using peak width. Island Arc. 23, 33-50.
Li, C.Z., 2007. Some recent advances in the understanding of the pyrolysis and gasification behaviour of Victorian brown coal. Fuel. 86, 1664–1683.
Li, X., Hayashi, J.I., Li, C.Z., 2006. FT-Raman spectroscopic study of the evolution of char structure during the pyrolysis of a Victorian brown coal. Fuel. 85, 1700-1707.
Li, X., Krooss, B.M., Weniger, P., Littke, R., 2015. Liberation of molecular hydrogen (H2) and methane (CH4) during non-isothermal pyrolysis of shales and coals: Systematics and quantification. International Journal of Coal Geology. 137, 152-164.
Liang, D., Guo, T., Chen, J., Bian, L., Zhao, Z., 2009. Some Progresses on Studies of Hydrocarbon Generation and Accumulation in Marine Sedimentary Regions, Southern China (Part 2): Geochemical Characteristics of Four Suits of Regional Marine Source Rocks, South China. Marine Origin Petroleum Geology. 14, 1-15.
Liu, D.H., Xiao, X.M., Tian, H., Min, Y., Zhou, Q., Cheng, P., Shen, J., 2013. Sample maturation calculated using Raman spectroscopic parameters for solid organics: Methodology and geological applications. Chin Sci Bull. 58, 1228-1241.
Liu, W., Liao, Y., Pan, Y., Jiang, B., Zeng, Q., Quan, S., Samuel, H.C., 2018. Use of ESI FT–ICR MS to investigate molecular transformation in simulated aerobic biodegradation of a sulfur-rich crude oil. Organic Geochemistry. 123, 17-26.
Lorant, F., Behar, F., 2002. Late generation of methane from mature kerogens. Energy & Fuels. 16, 412-427.
Loucks, R.G., Reed, R.M., Ruppel, S.C., Hammes, U., 2012. Spectrum of pore types and networks in mudrocks and a descriptive classification for matrix-related mudrock pores. Aapg Bulletin. 96, 1071-1098.
Lünsdorf, N.K., 2016. Raman spectroscopy of dispersed vitrinite - Methodical aspects and correlation with reflectance. International Journal of Coal Geology. 153, 75-86.
Lünsdorf, N.K., Dunkl, I., Schmidt, B.C., Rantitsch, G., von Eynatten, H., 2017. Towards a Higher Comparability of Geothermometric Data Obtained by Raman Spectroscopy of Carbonaceous Material. Part 2: A Revised Geothermometer. Geostandards and Geoanalytical Research. 41, 593-612.
Luo, Q., Hao, J., Skovsted, C.B., Luo, P., Khan, I., Wu, J., Zhong, N., 2017. The organic petrology of graptolites and maturity assessment of the Wufeng-Longmaxi Formations from Chongqing, China: Insights from reflectance cross-plot analysis. International Journal of Coal Geology. 183, 161-173.

Lupoi, J.S., Fritz, L.P., Parris, T.M., Hackley, P.C., Solotky, L., Eble, C.F., Schlaegle, S., 2017. Assessment of Thermal Maturity Trends in Devonian-Mississippian Source Rocks Using Raman Spectroscopy: Limitations of Peak-Fitting Method. Frontiers in Energy Research. 5.
Mackenzie, A.S., Brassell, S.C., Eglinton, G., Maxwell, J.R., 1982. Chemical Fossils: The Geological Fate of Steroids. Science. 217, 491-504.
Mackenzie, A.S., Hoffmann, C.F., Maxwell, J.R., 1981. Molecular parameters of maturation in the Toarcian shales, Paris Basin, France—III. Changes in aromatic steroid hydrocarbons. Geochimica Et Cosmochimica Acta. 45, 1345-1355.
Mahlstedt, N., Horsfield, B., Weniger, P., Misch, D., Shi, X., Noah, M., Boreham, C., 2022. Molecular hydrogen from organic sources in geological systems. Journal of Natural Gas Science and Engineering. 105, 104704.
Negri, F., Castiglioni, C., Tommasini, M., Zerbi, G., 2002. A Computational Study of the Raman Spectra of Large Polycyclic Aromatic Hydrocarbons:? Toward Molecularly Defined Subunits of Graphite [?]. Journal of Physical Chemistry A. 106, 3306-3317.
Noah, M., Horsfield, B., Han, S., Wang, C., 2020a. Precise maturity assessment over a broad dynamic range using polycyclic and heterocyclic aromatic compounds. Organic Geochemistry. 148, 104099.
Noah, M., Horsfield, B., Mahlstedt, N., Boreham, C.J., 2020b. Maturation characteristics of samples from Wallara-1 well, Canning Basin,as deduced from FT-ICR-MS analysis. Geoscience Australia, Canberra. Record 2020/58.
Pasteris, J.D., Wopenka, B., 1991. Raman spectra of graphite as indicators of degree of metamorphism. Canadian Mineralogist. 29, 1-9.
Peters, K.E., 1986. Guidelines for evaluating petroleum source rock using programmed pyrolysis. AAPG bulletin. 70, 318-329.
Peters, K.E., Moldowan, J.M., 1993. The Biomarker Guide: Interpreting Molecular Fossils in Petroleum and Ancient Sediments. Englewood Cliffs Nj Prentice Hall.
Pimenta, M., Dresselhaus, G., Dresselhaus, M.S., Cancado, L., Jorio, A., Saito, R., 2007. Studying disorder in graphite-based systems by Raman spectroscopy. Physical chemistry chemical physics. 9, 1276-1290.
Poetz, S., Horsfield, B., Wilkes, H., 2014. Maturity-Driven Generation and Transformation of Acidic Compounds in the Organic-Rich Posidonia Shale as Revealed by Electrospray Ionization Fourier Transform Ion Cyclotron Resonance Mass Spectrometry. Energy & Fuels. 28, 4877-4888.
Pusey, W., 1973. The esr-kerogen method. A new technique of estimating the organic maturity of sedimentary rocks. Petroleum Times. 1, 21-25.
Qi'an, M., Shun, Z., Guoxin, S., Xiuli, F., Chao, W., Yao, S., 2016. A seismic geomorphology study of the fluvial and lacustrine-delta facies of the Cretaceous Quantou-Nenjiang Formations in Songliao Basin, China. Marine and petroleum Geology. 78, 836-847.
Quirico, E., Rouzaud, J.N., Bonal, L., Montagnac, G., 2005. Maturation grade of coals as revealed by Raman spectroscopy: Progress and problems. Spectrochimica Acta Part a-Molecular and Biomolecular Spectroscopy. 61, 2368-2377.

Radke, M., 1982. Geochemical study on a well in the Western Canada Basin: relation of the aromatic distribution pattern to maturity of organic matter. Geochimica Et Cosmochimica Acta. 46, 1-10.
Reich, S., Thomsen, C., 2004. Raman spectroscopy of graphite. Philos Trans R Soc A. 362, 2271–2288.
Sadezky, A., Muckenhuber, H., Grothe, H., Niessner, R., Pöschl, U., 2005. Raman microspectroscopy of soot and related carbonaceous materials: Spectral analysis and structural information. Carbon. 43, 1731-1742.
Sanei, H., Haeri-Ardakani, O., Wood, J.M., Curtis, M.E., 2015. Effects of nanoporosity and surface imperfections on solid bitumen reflectance (BRo) measurements in unconventional reservoirs. International Journal of Coal Geology. 138, 95-102.
Santamaría-Orozco, D., Horsfield, B., Primio, R.D., Welte, D.H., 1998. Influence of maturity on distributions of benzo- and dibenzothiophenes in Tithonian source rocks and crude oils, Sonda de Campeche, Mexico. Organic Geochemistry. 28, 423-439.
Sauerer, B., Craddock, P.R., AlJohani, M.D., Alsamadony, K.L., Abdallah, W., 2017. Fast and accurate shale maturity determination by Raman spectroscopy measurement with minimal sample preparation. International Journal of Coal Geology. 173, 150-157.
Schenk, H., J., Horsfield, B., 1998. Using natural maturation series to evaluate the utility of parallel reaction kinetics models: an investigation of Toarcian shales and Carboniferous coals, Germany. Organic Geochemistry. 29, 137-154.
Schenk, H.J., Witte, E.G., Littke, R., Schwochau, K., 1990. Structural modifications of vitrinite and alginite concentrates during pyrolitic maturation at different heating rates. A combined infrared, 13C NMR and microscopical study. Organic Geochemistry. 16, 943-950.
Schenk, H.J., Witte, E.G., Müller, P., Schwochau, K., 1986. Infrared estimates of aliphatic kerogen carbon in sedimentary rocks. Organic Geochemistry. 10, 1099-1104.
Schito, A., Romano, C., Corrado, S., Grigo, D., Poe, B., 2017. Diagenetic thermal evolution of organic matter by Raman spectroscopy. Organic Geochemistry. 106, 57-67.
Schopf, J.W., Kudryavtsev, A.B., Agresti, D.G., Czaja, A.D., Wdowiak, T.J., 2005. Raman imagery: A new approach to assess the geochemical maturity and biogenicity of permineralized Precambrian fossils. Astrobiology. 5, 333-371.
Seifert, W.K., Moldowan, J.M., 1978. Applications of steranes, terpanes and monoaromatics to the maturation, migration and source of crude oils. Geochimica Et Cosmochimica Acta. 42, 77-95.
Seifert, W.K., Moldowan, J.M., 1980. Effect of thermal stress on source-rock quality as measured by hopane stereochemistry. Physics and Chemistry of The Earth. 12, 229-237.
Sonibare, O.O., Haeger, T., Foley, S.F., 2010. Structural characterization of Nigerian coals by X-ray diffraction, Raman and FTIR spectroscopy. Energy. 35, 5347-5353.
Sorokin, A.P., Malyshev, Y.F., Kaplun, V.B., Sorokina, A.T., Artemenko, T.V., 2013. Evolution and deep structure of the Zeya-Bureya and Songliao sedimentary basins (East Asia). Russian Journal of Pacific Geology. 7, 77-91.
Staplin, F., 1969. Sedimentary organic matter, organic metamorphism, oil and gas occurrences. Bull Canadian Petrol Geol. 17, 47-66.

Taylor, G.H., Teichmüller, M., Davis, A., Diessel, C., Robert, P., 1998. Organic Petrology. Borntraeger.
Teichmüller, M., Durand, B., 1983. Fluorescence microscopical rank studies on liptinites vitrinites in peat and coals and comparison with results of the Rock-Eval pyrolysis. International Journal of Coal Geology. 2, 197-230.
Tuinstra, F., Koenig, J.L., 1970. Raman Spectrum of Graphite. Journal of Chemical Physics. 53, 1126-1130.
Valentine, B.J., Hackley, P.C., Enomoto, C.B., Bove, A.M., Dulong, F.T., Lohr, C.D., Scott, K.R., 2014. Reprint of "Organic petrology of the Aptian-age section in the downdip Mississippi Interior Salt Basin, Mississippi, USA: Observations and preliminary implications for thermal maturation history". International Journal of Coal Geology. 136, 38-51.
Vandenbroucke, M., Largeau, C., 2007. Kerogen origin, evolution and structure. Organic Geochemistry. 38, 719-833.
Veld, H., Fermont, W.J., Jegers, L.F., 1993. Organic petrological characterization of Westphalian coals from The Netherlands: correlation between Tmax, vitrinite reflectance and hydrogen index. 20, 659-675.
Veld, H., Wilkins, R., Xianming, X., Buckingham, C., 1997. A fluorescence alteration of multiple macerals (FAMM) study of Netherlands coals with “normal” and “deviating” vitrinite reflectance. Organic Geochemistry. 26, 247-255.
Walters, C.C., Qian, K., Wu, C., Mennito, A.S., Wei, Z., 2011. Proto-solid bitumen in petroleum altered by thermochemical sulfate reduction. Organic Geochemistry. 42, 999-1006.
Wang, C., Feng, Z., Zhang, L., Huang, Y., Cao, K., Wang, P., Zhao, B., 2013. Cretaceous paleogeography and paleoclimate and the setting of SKI borehole sites in Songliao Basin, northeast China. Palaeogeography Palaeoclimatology Palaeoecology. 385, 17-30.
Wang, M., Li, Z., 2016. Thermal maturity evaluation of sedimentary organic matter using laser Raman spectroscopy. Acta Petrolei Sinica. 37, 1129-1136.
Wang, M., Xiao, X., Wei, Q., Zhou, Q., 2015. Thermal Maturation of Solid Bitumen in Shale as Revealed by Raman Spectroscopy. Natural Gas Geoscience. 26, 1712-1718.
Wei, H.H., Liu, J.L., Meng, Q.R., 2010. Structural and sedimentary evolution of the southern Songliao Basin, northeast China, and implications for hydrocarbon prospectivity. Aapg Bulletin. 94, 533-566.
Welte, D., Tissot, P., 1984. Petroleum Formation and Occurrence. Springer-verlag.
Wilkes, H., Clegg, H., Disko, U., Willsch, H., Horsfield, B., 1998a. Fluoren-9-ones and carbazoles in the Posidonia Shale, Hils Syncline, northwest Germany. 77, 657-668.
Wilkes, H., Disko, U., Horsfield, B., 1998b. Aromatic aldehydes and ketones in the Posidonia Shale, Hils Syncline, Germany. Organic Geochemistry. 29, 107-117.
Wu, L., Wang, P., Geng, A., 2019. Later stage gas generation in shale gas systems based on pyrolysis in closed and semi-closed systems. International Journal of Coal Geology. 206, 80-90.
Xiao, X., Wu, Z., 1995. Evaluation of Maturity of the Early Paleozoic Marine Hydrocarbon Source Rocks on the Basis of Organic Petrology. Acta Sedimentologica

751 Sinica. 013, 112-119.
752 Xiao, X., Zhou, Q., Cheng, P., Sun, J., Liu, D., Tian, H., 2020. Thermal maturation as
753 revealed by micro-Raman spectroscopy of mineral-organic aggregation (MOA) in
754 marine shales with high and over maturities. Science China Earth Sciences. 63, 1540-
755 1552.
756 Yang, S., Horsfield, B., 2020. Critical review of the uncertainty of Tmax in revealing
757 the thermal maturity of organic matter in sedimentary rocks. International Journal of
758 Coal Geology. 225, 103500.
759 Yang, W., He, S., Zhai, G., Tao, Z., Yuan, X., Wei, S., 2021. Maturity Assessment of the
760 Lower Cambrian and Sinian Shales Using Multiple Technical Approaches. Journal of
761 Earth Science. 32, 1262-1277.
762 Yui, T.F., Huang, E., Xu, J., 1996. Raman spectrum of carbonaceous material: a possible
763 metamorphic grade indicator for low-grade metamorphic rocks. J. Metamorph. Geol.
764 14, 115–124.
765 Zeng, F., Cheng, K., 1998. Solid 13C-NMR study on thermal evolution maturity of
766 lower palaeozoic carbonate rocks. Geology Geochemistry. 26, 9-15.
767 Zhang, Y., Li, Z., 2019. Raman spectroscopic study of chemical structure and thermal
768 maturity of vitrinite from a suite of Australia coals. Fuel. 241, 188-198.
769 Zhou, Q., Xiao, X., Pan, L., Tian, H., 2014. The relationship between micro-Raman
770 spectral parameters and reflectance of solid bitumen. International Journal of Coal
771 Geology. 121, 19-25.
772 Zhu, X., Shi, Q., Zhang, Y., Pan, N., Xu, C., Chung, K.H., Zhao, S., 2011.
773 Characterization of Nitrogen Compounds in Coker Heavy Gas Oil and Its Subfractions
774 by Liquid Chromatographic Separation Followed by Fourier Transform Ion Cyclotron
775 Resonance Mass Spectrometry. Energy & Fuels. 25, 281-287.

776